

Theory of linear sweep voltammetry with diffuse charge: unsupported electrolytes, thin films, and leaky membranes

David Yan^{a,*}, Martin Z. Bazant^b, Mary C. Pugh^c, Francis P. Dawson^a

^a*Department of Electrical and Computer Engineering, University of Toronto*

^b*Department of Chemical Engineering and Department of Mathematics, Massachusetts Institute of Technology*

^c*Department of Mathematics, University of Toronto*

Abstract

Linear sweep and cyclic voltammetry techniques are important tools for electrochemists and have a variety of applications in engineering. Voltammetry has classically been treated with the Randles-Sevcik equation, which assumes an electroneutral supported electrolyte. No general theory of linear-sweep voltammetry is available, however, for unsupported electrolytes and for other situations where diffuse charge effects play a role. In this paper, we provide a historical review of previous models and experiments and present a comprehensive mathematical theory of voltammetry in electrochemical cells with diffuse charge. We solve the time-dependent Poisson-Nernst-Planck (PNP) equations with generalized Frumkin-Butler-Volmer (FBV) boundary conditions, and show theoretical and simulated current-voltage curves for liquid and solid thin films, cells with blocking electrodes, and membranes with fixed background charge. The full range of dimensionless parameters is considered, including the dimensionless Debye screening length (scaled to the electrode separation), Damkohler number (ratio of characteristic diffusion and reaction times) and dimensionless sweep rate (scaled to the thermal voltage per diffusion time). The analysis focuses on the coupling of Faradaic reactions and diffuse charge dynamics, but capacitive charging of the double layers is also studied, for early time transients at reactive electrodes and for non-reactive blocking electrodes. Our results illustrate, in the context of voltammetry, which regimes can be approximated using simple analytical expressions and which require more careful consideration.

Keywords: Linear Sweep Voltammetry, Diffuse charge, Double layers, Frumkin-Butler-Volmer, Poisson-Nernst-Planck

1. Introduction

Polarography/linear sweep voltammetry (LSV)/cyclic voltammetry (CV) is the most common method of electro-analytical chemistry [1, 2, 3], pioneered by Heyrovsky and honored by a Nobel Prize in Chemistry in 1959. The classical Randles-Sevcik theory of polarograms is based on the assumption of diffusion limitation of the active species in

*Corresponding author: dyan@ele.utoronto.ca

a neutral liquid electrolyte, driven by fast reactions at the working electrode [4, 5, 6]. Extensions for slow Butler-Volmer kinetics (or other reaction models) are also available [1]. The half-cell voltage is measured at a well-separated reference electrode in the bulk liquid electrolyte, which is assumed to be electro-neutral, based on the use of a supporting electrolyte [7].

In many electrochemical systems of current interest, however, the electrolyte is unsupported, doped, or strongly confined by electrodes with nanoscale dimensions. Examples include super-capacitors, [8], capacitive deionization [9], pseudo-capacitive deionization and energy storage [10, 11], electrochemical thin films [12, 13, 14, 15], solid electrolytes used in Li-ion/Li-metal [16, 17], electrochemical breakdown of integrated circuits [18], fuel cells [19, 20], nanofluidic systems [21, 22, 23], electrodialysis [24, 25, 26], and charged porous “leaky membranes” [27, 28] for shock electrodialysis [29, 30] and shock electrodeposition [31, 32]. In all of these situations, diffuse ionic charge must play an important role in voltammetry, which remains to be fully understood.

Despite an extensive theoretical and experimental literature on this subject (reviewed below), to the authors’ knowledge, there has been no comprehensive mathematical modeling of the effects of diffuse charge on polarograms, while fully taking into account time-dependent electromigration and Frumkin effects of diffuse charge on Faradaic reaction rates. The goal of this work is thus to construct and solve a general model for voltammetry for charged electrolytes. We consider the simplest Poisson-Nernst-Planck (PNP) equations for ion transport for dilute liquid and solid electrolytes and leaky membranes, coupled with “generalized” Frumkin-Butler-Volmer (FBV) kinetics for Faradaic reactions at the electrodes [12, 33, 34, 35, 36, 37], as reviewed by Biesheuvel, Soestbergen and Bazant [14] and extended in subsequent work [10, 11, 15]. Unlike most prior analyses, however, we make no assumptions about the double layer thickness, Stern layer thickness, sweep rate, or reaction rates in numerical solutions of the full PNP-FBV model. We also define a complete set of dimensionless parameters and take various physically relevant limits to obtain analytical results whenever possible, which are compared with numerical solutions in the appropriate limits.

The paper is structured as follows. We begin with a review of theoretical and experimental studies of diffuse-charge effects in voltammetry in Section 2. The PNP-FBV model equations are formulated and cast in dimensionless form in Section 3, followed by voltammetry simulations on a single electrode in a supported and unsupported electrolyte in Section 4. In Section 5, ramp voltages are applied to systems with one or two blocking electrodes, and simulation results are used to compare simulated and theoretical capacitance curves. Sections 6 and 7 show simulations on electrochemical thin films, considering both the thin and thick double layer limits. Finally, we simulate ramped voltages applied to porous “leaky” membranes with fixed background charge in Section 8, and conclude with a brief outlook for future work.

2. Historical Review

The modeling of diffuse charge dynamics in electrochemical systems has a long history, reviewed by Bazant, Thornton and Ajdari [38]. Frumkin [39] and Levich [40] are credited with pointing out the need to consider effects of diffuse charge on Butler-Volmer reaction kinetics at electrodes in unsupported electrolytes, although complete mathematical models for dynamical situations were not formulated until much later. In electrochemical

impedance spectroscopy (EIS) [41], it is well known that the double-layer capacitance must be considered in parallel with the Faradaic reaction resistance in order to describe the interfacial impedance of electrodes. Since the pioneering work of Jaffé [42, 43] for semiconductors and Chang and Jaffé for electrolytes [44], Macdonald [45, 46] and others have formulated microscopic PNP-based models using the Chang-Jaffé boundary conditions [47], which postulate mass-action kinetics, proportional to the active ion concentration at the surface. This approximation includes the first “Frumkin correction”, i.e. the jump in active species concentration across the double layer, but not the second, related to the jump in electric field that drives electron transfer at the surface [12, 14]. More importantly, all models used to interpret EIS measurements, whether based on microscopic transport equations or macroscopic equivalent circuit models, only hold for the linear response to an infinitesimal sinusoidal applied voltage or current.

The *nonlinear* coupling of diffuse charge dynamics with Faradaic reaction kinetics has received far less attention and, until recently, has been treated mostly by empirical macroscopic models, as reviewed by Biesheuvel, Soestbergen and Bazant [14]. Examples of *ad hoc* approximations include fixing the electrode charge or zeta potential, independently from the applied current or voltage, and assuming a constant double layer capacitance in parallel with a variable Faradaic reaction resistance given by the Butler-Volmer equation. Such empirical models are theoretically inconsistent, because the electrode charge and double-layer capacitance are not constant independent variables to be fitted to experimental data. Instead, the microscopic model must include a proper electrostatic boundary condition, relating surface charge to the jump in the normal component of the Maxwell dielectric displacement [48], and the Butler-Volmer equation, or another reaction-rate model, must be applied at the same position (the “reaction plane”). This inevitably leads to nonlinear dependence of the electrode surface charge on the local current density [10, 12], which includes both Faradaic current from electron-transfer reactions and Maxwell displacement current from capacitive charging [35, 38, 49].

Interest in voltammetry in low conductivity solvents and dilute electrolytes without little to no supporting electrolyte has slowly grown since the 1970s. Since the work of Buck [50], a variety of PNP-based microscopic models have been proposed [51, 52, 53, 54], which provide somewhat different boundary conditions than the FBV model described below. Since the 1980s, various experiments have focused on the role of supporting electrolyte [2]. For example, Bond and co-workers performed linear sweep [55] and cyclic [56, 57] voltammetry using the ferrocene oxidation reaction on a microelectrode while varying supporting electrolyte concentrations. One of the primary theoretical concerns at that time was modeling the extra ohmic drop in the solution from the electromigration effects which entered into the physics due to low supporting electrolyte concentration. Bond [58] and Oldham [59] both solved the PNP equations for steady-state voltammetry in dilute solutions with either Nerstian or Butler-volmer reaction kinetics to obtain expressions for the ohmic drop. While they listed the full PNP equations, they analytically solved the system only with the electroneutrality assumption or for small deviations from electroneutrality, which is a feature of many later models as well [60, 61, 54]. The bulk electroneutrality approximation is generally very accurate in macroscopic electrochemical systems [7, 62], although care must be taken to incorporate diffuse charge effects properly in the boundary conditions, as explained below. Bento, Thouin and Amatore [63, 64] continued this type of experimental work on voltammetry and studied the effect of diffuse layer dynamics and migrational effects in electrolytes with low support. They also per-

formed voltammetry experiments on microelectrodes in solutions while varying the ratio of supporting electrolyte to reactant, and noted shifts in the resulting voltammograms and a change in the solution resistance [65].

More recently, Compton and co-workers have done extensive work involving theory [66, 67, 68], simulations [66, 69, 70, 37] (and see Chapter 7 of [3] or Chapter 10 of [2]) and experiments [71, 72, 73, 74] on the effect of varying the concentration of the supporting electrolyte on voltammetry. Besides considering a different (hemispherical) electrode geometry motivated by ultramicroelectrodes [75], there are two significant differences between this body of work and ours, from a modeling perspective.

The first difference lies in the treatment of the supporting electrolyte. The main positive ion that takes part in the species is denoted by A, and the supporting electrolyte as MX, where M is the positive species and X is the negative species. There are two cases for the other part of the reaction: either there is a negative ion [66, 70] or neutral molecule (that does not dissociate) which takes part in the reaction [71, 72], species B. For the latter case, the negative supporting ion X takes up the role of the co-ion, and extra concentration of species X is added to balance species A. Modeling of uncharged and supporting ionic species has also been a feature of older models in the literature [58, 59, 60]. In this work, we only consider the two extremes: either an unsupported binary electrolyte or (briefly, for comparison) a classical fully supported electrolyte.

The second difference lies in treatment of specific adsorption of ions and a related approximation used to simplify the full model. Although some studies involve numerical solutions of the full PNP equations with suitable electrostatic and reaction boundary conditions [37], many others employ the “zero-field approximation” for the thin double layers [37, 69], which is motivated by strong specific adsorption of ions. In this picture, the Stern layer [76] (outside the continuum region of ion transport) is postulated to have two parts: a outer layer of adsorbed ions that fully screens the surface charge, and an inner uncharged dielectric layer that represents solvent molecules on the electrode surface. The assumption of complete screening motivates imposing a vanishing normal electric field as the boundary condition for the neutral bulk electrolyte at the electrode outside the double layers. This assertion also has the effect of eliminating the electromigration term from the flux entering the double layers, despite the inclusion of this term in the bulk mass flux. Physically, this model assumes that the electrode always remains close to the potential of zero charge, even during the passage of transient large currents.

Here, we base our analysis on the PNP equations with “generalized FBV” boundary conditions [14, 15], to describe Faradaic reactions at a working electrode, whose potential is measured relative to the point of zero charge, in the absence of specific adsorption of ions. The model postulates a charge-free Stern layer of constant capacitance, whose voltage drop drives electron transfer according to the Butler-Volmer equation, where the exchange current is determined by the local concentration of active ions at the reaction plane. This approach was perhaps first introduced by Itskovich, Kornyshev and Vorontyntsev [33, 34] in the context of solid electrolytes, with one mobile ionic species and fixed background charge. For general liquid or solid electrolytes, the FBV model based on the Stern boundary condition was perhaps first formulated by Bazant and co-workers [12, 14, 35] and independently developed by He et al. [36] and Streeter and Compton [37]. The FBV-Stern model was extended to porous electrodes and multicomponent electrolytes by Biesheuvel, Fu and Bazant [10, 11].

Most of the literature on modeling diffuse-charge effects in electrochemical cells has

focused on either linear AC response (impedance) or nonlinear steady-state response (differential resistance), with a few notable exceptions. The PNP-FBV model was apparently first applied to chronoampereometry (response to a voltage step) by Streeter and Compton [37] and to chronopotentiometry (response to a current step) by Soestebergen, Biesheuvel and Bazant [49], each in the limit of thin double layers for unsupported binary liquid electrolytes. Here, we extend this work to voltammetry and consider a much wider range of conditions, including thick double layers, fixed background charge, and slow reactions.

It is important to emphasize the generality of the PNP-FBV framework, which is not limited to thin double layers and stagnant neutral bulk electrolytes. Chu and Bazant [13] analyzed the model for a binary electrolyte under extreme conditions of over-limiting current, where the double layer loses its quasi-equilibrium structure and expands into an extended bulk space charge layer, and performed simulations of steady transport across a thin film at currents over 25 times the classical diffusion-limited current (which might be achieved in solid, ultra-thin films). Transient space charge has also been analyzed in this way for large applied voltages, for both blocking electrodes [38, 77] and FBV reactions [49]. A validation of the PNP-FBV theory was recently achieved by Soestbergen [78], who fitted the model to experimental data of LeMay and workers for planar nano-cavities [79, 80]. The FBV model has also been applied to nonlinear “induced-charge” electrokinetic phenomena [81], in the asymptotic limit of thin double layers. Olsen, Bruus and Ajdari [82, 83] used the quasi-equilibrium FBV double-layer model in a theory of AC electro-osmotic flow over micro-electrode arrays. Moran and Posner [84] applied the same approach to reaction-induced-charge-electrophoresis of reactive metal colloidal particles in electric fields [85].

Many of these recent studies have exploited effective boundary conditions for thin double layers, which were systematically derived by asymptotic analysis and compared to full solutions of the PNP equations, rather than *ad hoc* approximations. Matched asymptotic expansions were first applied to steady-state PNP transport in the 1960s without considering FBV reaction kinetics [86, 87, 88, 89] and used extensively in theories of ion transport [24] and electro-osmotic fluid instabilities [90, 91] in electrodialysis, involving ion-exchange membranes rather than electrodes. Baker and Verbrugge [92] analyzed a simplified problem with fast reactions, where the active species concentration vanishes at the electrode. Bazant and co-workers first used matched asymptotic expansions to treat Faradaic reactions using the PNP-FBV framework, applied to steady conduction through electrochemical thin films [12, 13]. Richardson and King [93] extended this approach to derive effective boundary conditions for time-dependent problems, which provides rigorous justification for subsequent studies of transient electrochemical response using the thin double layer approximation, including ours.

Finally, for completeness, we note that Moya et al. [94] recently analyzed a model of double-layer effects on LSV for the case of a neutral electrolyte surrounding an ideal ion-exchange membrane with thin quasi-equilibrium double layers, and no electrodes with Faradaic reactions to sustain the current.

3. Mathematical Model

3.1. Poisson-Nernst-Planck Equations for Ion Transport

The Nernst-Planck equation for ions in the bulk ($X \in (0, L)$) is

$$\frac{\partial C_{\pm}}{\partial \tau} = -\frac{\partial}{\partial X} \left[-\frac{z_{\pm} D_{\pm} F}{RT} C_{\pm} \frac{\partial \Phi}{\partial X} - D_{\pm} \frac{\partial C_{\pm}}{\partial X} \right] \quad (1)$$

where $C_{\pm}(X, \tau)$ denotes the cation and anion concentrations and z_{\pm} is the charge number, where we take the convention that the sign of the charge is attached to z_- . D_{\pm} is the diffusivity of the positive and negative ions, and F and R are Faraday's constant and the ideal gas constant, respectively.

The potential $\Phi(X, \tau)$ is determined by Poisson's equation:

$$-\varepsilon_s \frac{\partial^2 \Phi}{\partial X^2} = F (z_+ C_+ + z_- C_-) \quad (2)$$

where ε_s is the bulk permittivity of the electrolyte.

We will be considering binary electrolytes in this work, and equations (1)-(2) describe a system with two mobile charges. For a solid electrolyte with fixed countercharge, we may set $C_-(X, \tau) = C_0$ and only solve one diffusion equation. Note that this classical first approximation [34] neglects excluded volume effects on a lattice ("crowding"), which are important in crystalline ionic solids [95] and ion insertion electrodes [96] especially at high voltages [81]. The model might be better for polymeric solid electrolytes with less severe volume constraints, or for doped solid crystals with low carrier concentrations at sufficiently low voltages. For a 'leaky membrane' [27], we add a constant background charge ρ_s to equation (2),

$$-\varepsilon_s \frac{\partial^2 \Phi}{\partial X^2} = F (z_+ C_+ + z_- C_- + \rho_s) \quad (3)$$

Finally, for a supported electrolyte, we set $\Phi(X, \tau) = 0$ and only solve the two Nernst-Planck equations for each charged species.

3.2. Frumkin-Butler-Volmer Boundary Conditions for Faradaic Reactions

We use the generalized Frumkin-Butler-Volmer (FBV) equation,

$$\mp \left(-\frac{z_+ D F}{RT} \frac{\partial \Phi}{\partial X} - D_+ \frac{\partial C_+}{\partial X} \right) \Big|_{X=0, L} = K_O C_+ e^{\left(\frac{-\alpha_a n F \Delta \Phi}{RT} \right)} - K_R C_M e^{\left(\frac{\alpha_c n F \Delta \Phi}{RT} \right)}. \quad (4)$$

to model Faradaic reactions at an electrode, such as the electrodeposition reaction



where the \mp in equation (4) varies depending on whether the boundary condition is applied at the left or right boundary and $n = z_+$ is the number of electrons transferred to reduce the cation to the metallic state M . K_O and K_R are the reaction rate parameters. In the case of a blocking, or ideally polarizable electrode, or for a species which does not take part in the electrode reaction, $K_O = K_R = 0$. Following [15] and other models

using the FBV equation, $\Delta\Phi$ is explicitly defined as being across the Stern layer (and always as the potential at the electrode minus the potential at the Stern plane).

The boundary condition on Φ at an electrode is

$$\mp\lambda_s \frac{\partial\Phi}{\partial X} = \Delta\Phi \quad (5)$$

where again the sign \mp is for the left hand and right side electrode and λ_s is the effective width of the Stern layer, allowing for a different (typically lower) dielectric constant [12, 35]. In this model, the point of zero charge (pzc) occurs when $\Delta\Phi = 0$ across the Stern layer, so the potential of the working electrode is defined relative to pzc. For a more general model with two electrode having different pzc, an additional potential shift must be added to (5) at least one electrode [36, 37].

In this work, we will be considering the effect of a ramped voltage at the right side electrode, which means an applied voltage

$$V(\tau) = S\tau \quad (6)$$

where S is the voltage scan or sweep rate.

The system of equations is closed with a current conservation equation,

$$\frac{d\Phi_X(L, \tau)}{d\tau} = -\frac{1}{\varepsilon_s} \left\{ J(\tau) - F \left[K_O C_+(L, \tau) e^{(-\alpha_a n F \Delta\Phi)} - K_R C_M e^{(\alpha_c n F \Delta\Phi)} \right] \right\} \quad (7)$$

For some simulations in this work, we wish to model only one electrode, with the other approximating an ideal reference electrode or an ideal reservoir. In this case, we use the electrode at $X = L$ as the electrode under test, and use the boundary conditions

$$C_{\pm}(0, \tau) = C_0, \quad \Phi(0) = 0 \quad (8)$$

at $X = 0$, where C_0 is a reference concentration.

3.3. Dimensionless Equations

It is convenient to rescale the PNP equations so that distance, time, concentration and potential are scaled to device thickness, the diffusion time scale, a reference concentration and the thermal voltage, respectively:

$$x \equiv \frac{X}{L}, \quad t \equiv \frac{D\tau}{L^2}, \quad c_{\pm} \equiv \frac{C_{\pm}}{C_0}, \quad \phi \equiv \frac{F\Phi}{RT}. \quad (9)$$

Rescaling the Poisson-Nernst-Planck equations (1)–(2) yields the dimensionless equations (assuming a 1:1 electrolyte, $z_+ = -z_- = 1$ and assuming $D_+ = D_- = D$)

$$\frac{\partial c_{\pm}}{\partial t} = -\frac{d}{dx} \left[\mp c_{\pm} \frac{\partial \phi}{\partial x} - \frac{\partial c_{\pm}}{\partial x} \right] \quad (10)$$

$$-\epsilon^2 \frac{\partial^2 \phi}{\partial x^2} = \frac{1}{2} (c_+ - c_-) \quad (11)$$

where $\epsilon = \lambda_D/L$ is the ratio between the Debye length $\lambda_D \equiv \sqrt{\frac{\varepsilon_s RT}{2F^2C_0}}$ and L . To nondimensionalize the boundary conditions, the following rescaled parameters are introduced

$$k_c = \frac{K_O L}{4D}, \quad j_r = \frac{K_R L C_M}{4DC_0}, \quad \delta = \frac{\lambda_s}{\lambda_D} \quad (12)$$

so that equation (4) becomes (assuming $\alpha_a = \alpha_c = 1/2$)

$$\mp \left(-c_+ \frac{\partial \phi}{\partial x} - \frac{\partial c_+}{\partial x} \right) \Big|_{x=0,1} = 4k_c c_+ e^{-\Delta\phi/2} - 4j_r e^{\Delta\phi/2} \quad (13)$$

Equation (5) rescales to

$$\mp \epsilon \delta \phi_x = \Delta\phi \quad (14)$$

and finally, equation (7) becomes

$$-\frac{\epsilon^2}{2} \frac{d}{dt} \phi_x(1, t) = j - \left[k_c c_+(1, t) e^{-\Delta\phi/2} - j_r e^{\Delta\phi/2} \right] \quad (15)$$

where j is scaled to the limiting current density $J_{\text{lim}} = \frac{4FDC_0}{L}$.

The rescaled equations contain two fundamental time scales: the diffusion time scale, $\tau_D = L^2/D$ and the reaction time scale, $\tau_R = L/K$, for a characteristic reaction rate K . There is also the imposed voltage scan rate time scale, $\tau_S = \frac{RT}{F}/S$. The ratios of these three time scales result in two dimensionless groups: the nondimensional voltage scan rate,

$$\tilde{S} = \frac{\tau_D}{\tau_S} = \frac{SL^2F}{DRT} \quad (16)$$

and the nondimensional reaction rate,

$$k = \frac{\tau_D}{4\tau_R} = \frac{KL}{4D} \quad (17)$$

also known as the “Damkohler number”. In Eq. (12), the latter takes two forms, $k = k_c$ and $k = j_r$, for the forward (oxidation) and backward (reduction) reactions with the characteristic rates, $K = K_O$ and $K = K_R C_M/C_0$, respectively.

The dimensionless model also contains thermodynamic information about the electrochemical reaction, independent of the overall reaction rate [96, 1, 10]. For any choice of a single reaction-rate scaling, then there is a third dimensionless group, which can be expressed as the (logarithm of) the ratio of the dimensionless forward and backward reaction rates,

$$\ln \frac{k_c}{j_r} = \ln \frac{K_0 C_0}{K_R C_M} = \Delta\phi^\Theta \quad (18)$$

This is the dimensionless equilibrium interfacial voltage, where the net Faradaic current (equation (13)) vanishes in detailed balance between the oxidation and reduction reactions for the reactive cation at the bulk reference concentration C_0 .

3.4. Limits of Interest

3.4.1. Thin Double Layers

The dimensionless parameters ϵ and δ control how the model handles the double layer and diffuse charge dynamics respectively. ϵ governs double layer thickness relative to device thickness, whereas δ , which is effectively a ratio of Stern and diffuse layer capacitance, controls the competition between the Stern and diffuse layers in overall double layer behavior. The limit of ambipolar diffusion corresponds to $\epsilon \rightarrow 0$. In this limit, equation (11) is simply

$$c_+ = c_- \quad (19)$$

which means that the two ionic transport equations (equation (10)) simplify to a single diffusion equation,

$$\frac{\partial c}{\partial t} = \frac{\partial^2 c}{\partial x^2} \quad (20)$$

and the potential is calculated via

$$\frac{\partial}{\partial x} \left(c \frac{\partial \phi}{\partial x} \right) = 0 \quad (21)$$

There are also two limits of interest on δ . The first is the “Gouy-Chapman” (GC) limit, $\delta \rightarrow 0$, which corresponds to a situation where all of the potential drop in the double layer is across the diffuse region, and the second is the “Helmholtz” (H) limit, $\delta \rightarrow \infty$, where all of the potential drop is across the Stern layer. In the former case, the Boltzmann distribution for ions is invoked ($c_{\pm} = \exp(\mp \Delta\phi_D)$) and the right hand side of equation (13) becomes

$$\text{Flux} = 4k_c c_+ e^{-\Delta\phi_D} - 4j_r \quad (22)$$

where $\Delta\phi_D$ is the potential drop across the diffuse region. In the latter case, the right hand side of equation (13) becomes

$$\text{Flux} = 4k_c c_+ e^{-\Delta\phi_S/2} - 4j_r e^{\Delta\phi_S/2} \quad (23)$$

where $\Delta\phi_S$ is the potential drop across the Stern layer.

3.4.2. Fast Reactions

The most common approximation for the boundary conditions in voltammetry is the Nernstian limit of fast reactions, $k_c, j_r \rightarrow \infty$, for a fixed ratio, j_r/k_c , corresponding to a given equilibrium half-cell potential for the reaction, Eq. (18). In this limit, the left-hand sides of equations (13) and (22)–(23) approach zero, and all three boundary conditions reduce to the Nernst equation,

$$\Delta\phi = \Delta\phi^{\Theta} + \ln c_+ \quad (24)$$

where again the bulk solution is used as the reference concentration. In order to place the Nernst equation in the standard form [1, 96],

$$E = \frac{RT}{nF} \Delta\phi^{\text{eq}} = E^{\Theta} + \frac{RT}{nF} \ln \frac{C_+}{C_{\text{ref}}} \quad (25)$$

we must define the equilibrium interfacial voltage relative to a standard reference electrode (e.g. the Standard Hydrogen Electrode in aqueous systems at room temperature and atmospheric pressure with $C_{\text{ref}} = 1 \text{ M}$) by shifting the reference potential,

$$E^{\Theta} = \frac{RT}{nF} \left(\Delta\phi^{\Theta} - \ln \frac{C_0}{C_{\text{ref}}} \right) = \frac{RT}{nF} \ln \frac{K_0 C_{\text{ref}}}{K_R C_M} \quad (26)$$

In this way, tables of standard half-cell potentials can be used to determine the ratio of reaction rate constants, and measurements of exchange current density can then determine the individual oxidation and reduction rate constants.

3.5. Numerical Method

In space, we use a three-point variable mesh size finite difference scheme. In time, we use a variable step size implicit-explicit backwards differencing formula (VSSBDF2) published by Wang and Ruuth [97, 98]. We use an adaptive time stepper with error control, with the time stepping method to be covered in a follow up work. All simulations were performed using MATLAB running on Debian Linux with 16 cores and 64 GB of RAM.

4. Bulk Liquid Electrolytes

4.1. Model Problem

The model problem for this section is a single electrode in an aqueous electrolyte with a reference electrode at $x = 0$ and two mobile ions. Voltammetry on a single electrode in solution is one of the oldest problems in electrochemistry; experiments are usually conducted using the “three-electrode setup” shown in Figure 1,

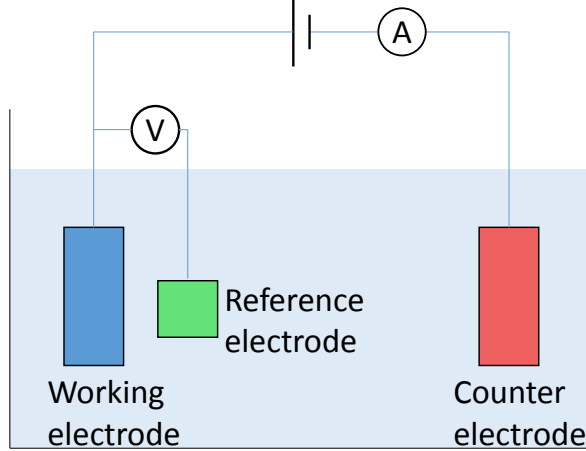


Figure 1: Three-electrode setup in an electrolyte, which is commonly used for voltammetry experiments. Running current through an electrode polarizes it, and so the “counter electrode” is used to provide current, while the “reference electrode” is used as a voltage reference.

where one electrode acts as a voltage reference while another (the auxillary electrode) provides current. Computationally, this setup can be mimicked with

$$C_{\pm}(0, \tau) = C_0, \quad \Phi(0) = 0 \quad (27)$$

at $X = 0$, where C_0 is a reference concentration. This models a cell with only one electrode, with the other approximating an ideal reference electrode or an ideal reservoir.

In order to ensure that dynamics do not reach the reference electrode, we restrict ourselves to the regime $\tilde{S} \gg 1$ and $t \ll 1$. The reaction rate parameter k can either be $\gg 1$ or $\ll 1$, which correspond to a diffusion-limited regime and reaction-limited regime, respectively.

4.2. Supported Electrolytes

A supported electrolyte is where an inert (does not take part in electrode or bulk reactions) salt is added in order to screen the electric field so as to render electromigration effects negligible (i.e. $\phi = 0$ in the bulk). Voltammetry with supported electrolytes has classically been treated as a semi-infinite diffusion problem. For an aqueous system at a planar electrode with a reversible electrode reaction (reaction much faster than diffusion) involving two species denoted O (oxidized) and R (reduced), the diffusion equations are given, using the present notation, by (see Chapters 5 and 6 of [1])

$$\frac{\partial C_O(X, \tau)}{\partial \tau} = D_O \frac{\partial^2 C_O(X, \tau)}{\partial X^2}, \quad \frac{\partial C_R(X, \tau)}{\partial \tau} = D_R \frac{\partial^2 C_R(X, \tau)}{\partial X^2}, \quad (28)$$

where D_O and D_R are the diffusivities of the respective species, with the initial conditions

$$C_O(X, 0) = C_O^*, \quad C_R(X, 0) = 0, \quad (29)$$

where C_O^* is a reference concentration. The boundary conditions are

$$\lim_{X \rightarrow \infty} C_O(X, \tau) = C_O^*, \quad \lim_{X \rightarrow \infty} C_R(X, \tau) = 0, \quad (30)$$

with a flux balance boundary condition at the electrode,

$$D_O \left(\frac{\partial C_O(X, \tau)}{\partial X} \right)_{X=0} = D_R \left(\frac{\partial C_R(X, \tau)}{\partial X} \right)_{X=0}, \quad (31)$$

and finally a Nernstian reaction boundary condition which assumes rapid charge kinetics,

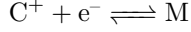
$$\frac{C_O(0, \tau)}{C_R(0, \tau)} = \exp \left[\frac{nF}{RT} (V(\tau) - V_0') \right], \quad (32)$$

where $V(\tau) = V_0 + S\tau$ and V_0' are the applied and equilibrium electrode potentials, respectively, S is the scan rate, and the other constants take their usual meanings. This system of equations can be solved to find the resulting current density,

$$J(\tau) = nFD_O \left(\frac{\partial C_O(X, \tau)}{\partial X} \right)_{X=0} = nFAC_O^* (\pi D_O \sigma)^{\frac{1}{2}} \chi(\sigma\tau), \quad (33)$$

where $\sigma \equiv nFS/RT$ and χ is the Randles-Sevcik function. The same system of equations is also often considered for irreversible (slow reactions compared to diffusion) and ‘quasi-reversible’ reactions, with the appropriate changes to the boundary conditions (31)–(32).

The reaction we will be considering is



where M represents the electrode material. An example of such a reaction is the Cu-CuSO₄ electrodeposition process. Since the reaction only involves one of the two ions as opposed to both as in the Randles-Sevcik case, the mathematics are simplified somewhat and we are able to obtain an analytical solution. We need to solve the diffusion equation (equation (20)) on $x \in (0, \infty)$ with the fast reaction boundary condition, equation (24) with $\Delta\phi = v(t)$. The applied voltage is $v(t) = -\tilde{S}t$ since we consider positive current as out of the electrode, and the current is computed via $j = \frac{\partial c}{\partial x} \big|_{x=0}$. Using a Laplace transform and Duhamel’s principle, we arrive at the solution

$$j(t) = \sqrt{\tilde{S}} e^{-\tilde{S}t} \operatorname{erfi}(\sqrt{\tilde{S}}t) \quad (34)$$

where $\operatorname{erfi}(z) = \frac{2}{\sqrt{\pi}} \int_0^z \exp x^2 dx$ is the imaginary error function. The derivation can be found in Appendix A. We term equation (34) a “modified” Randles-Sevcik equation, which applies to voltammetry on a fast reaction involving only one ionic species in a supported electrolyte. Figure 2 shows simulated $j(t)$ curves with various values of k compared to equation (34), with $\tilde{S} = 50$.

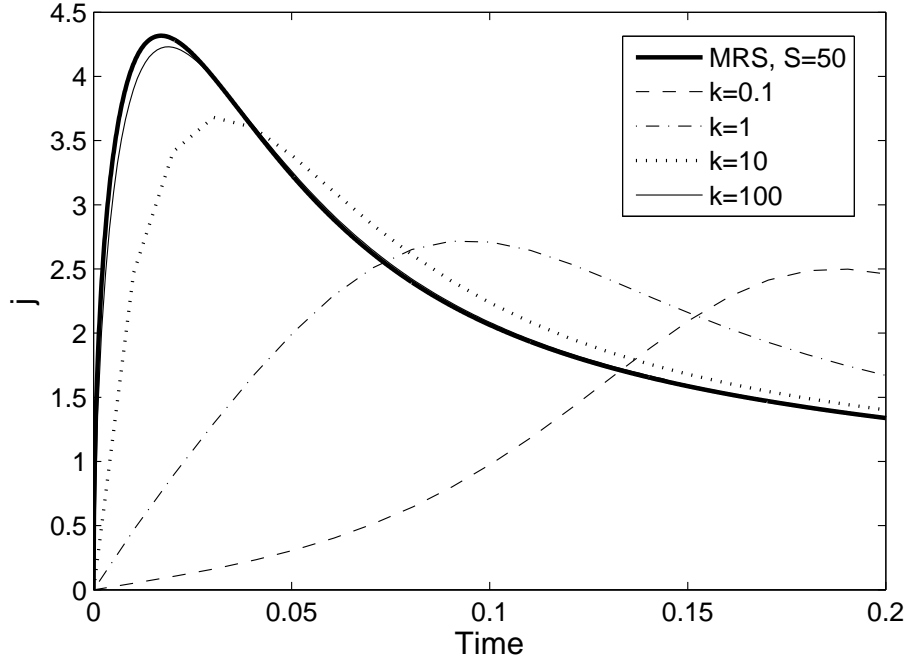


Figure 2: Simulated current curves for a supported electrolyte with one electrode in response to a voltage ramp with $\tilde{S} = -50$, with various values of k . Also shown is the high reaction rate limit in equation (2).

The simulated curves in Figure 2 approach equation (34) in the limit of large k , which makes equation (34) a good approximation for the current response to a ramped voltage in a supported electrolyte with fast, single-species reaction. Note that due to definition differences, the simulated current must be multiplied by 4 because there is a difference of a factor of 4 between the current in equation (15) and the ion flux in equation (13).

4.3. Unsupported Electrolytes with Thin Double Layers

For the single-electrode, thin-EDL, unsupported electrolyte problem, we use a value of $\epsilon = 0.001$, and impose the restrictions $\tilde{S} \gg 1$ and $t \ll 1$ in order to remain in a diffusion-limited regime. Figure 3 shows plots of voltammograms for $v(t) = -50t$ ($\tilde{S} = 50$) with $\delta = 100$, and the modified Randles-Sevcik plot also shown for comparison. The $k = 50$ simulation gives results which are numerically equivalent to the large k limit.

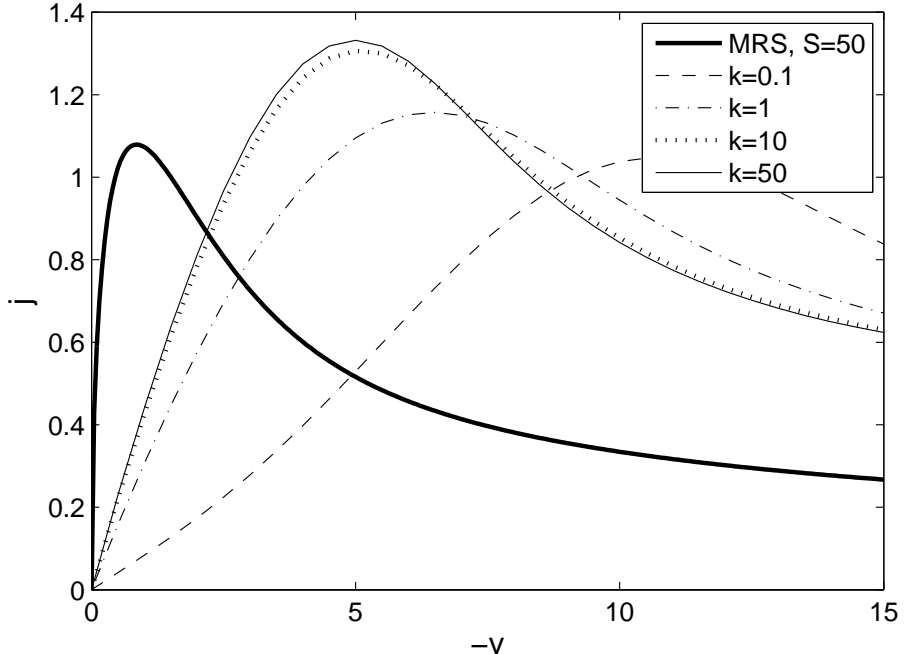


Figure 3: Simulated j vs. v curves with various values of reaction rate k for an unsupported electrolyte with one electrode, in response to a ramped voltage with scan rate $\tilde{S} = -50$. The $k = 50$ simulation gives results which are numerically equivalent to the large k limit. Also shown is the theoretical result for a supported electrolyte from equation 2.

It is interesting to note that, while the situations leading to the currents in Figures 2 and 3 may seem superficially similar (both involve voltammetry on a single electrode with fast reactions), they do not produce the same results. The physical difference is that electromigration is included in the latter (so equation (11) is solved along with the anion transport equation), which opposes diffusion, resulting in a slower response. This type of shift in the voltammogram for low support has been well documented in the experimental literature (see [55, 63, 64, 70, 72], among others).

Next, Figures 4 and 5 show the voltammograms for the $k = 0.1$ (reaction limited) and $k = 50$ (diffusion limited) cases, with accompanying concentration profiles (c_+ and c_- are identical in the bulk but only c_+ is shown). The current in Figure 4 exhibits the initial exponential shape and slower response indicative of reaction limited dynamics compared to Figure 5.

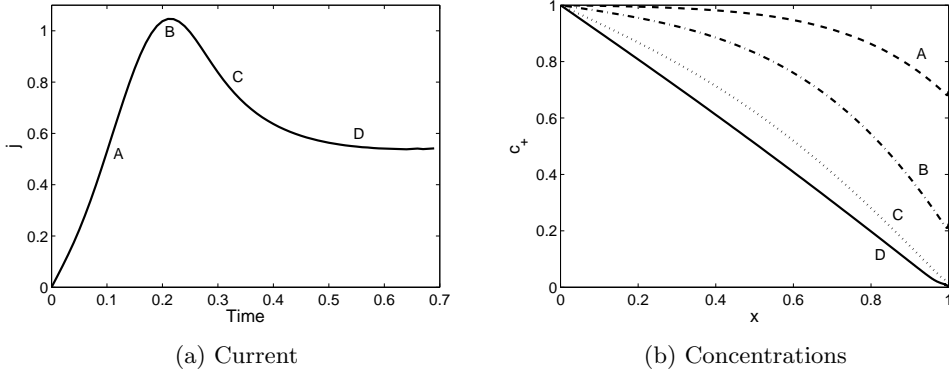


Figure 4: (a) Voltammogram and (b) concentrations with $k = 0.1$ (reaction limited) for an unsupported electrolyte with one electrode subjected to a ramped voltage with scan rate $\tilde{S} = 50$, with $\epsilon = 0.001$ and $\delta = 100$. Labels in the concentration plot correspond to snapshots of cation concentration c_+ at times labeled on the current vs. time plot.

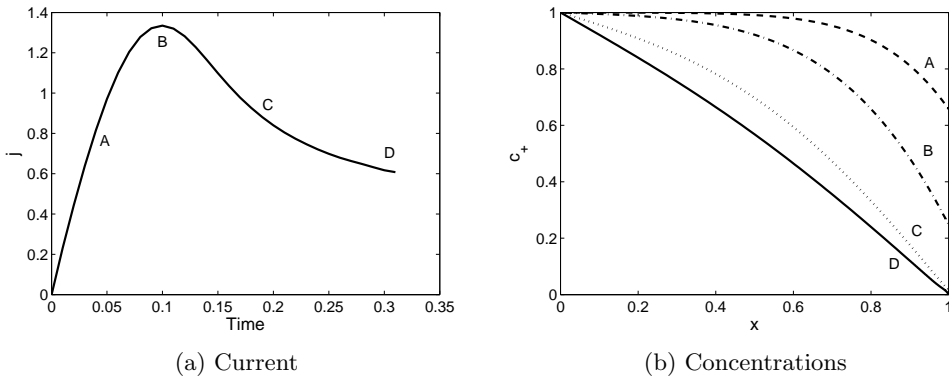


Figure 5: (a) Voltammogram and (b) concentrations with $k = 100$ (diffusion limited) for an unsupported electrolyte with one electrode subjected to a ramped voltage with scan rate $\tilde{S} = -50$, with $\epsilon = 0.001$ and $\delta = 100$. Labels in the concentration plot correspond to snapshots of cation concentration c_+ at times labeled on the current vs. time plot.

Finally, Figure 6 shows two voltammetry cycles on the system with $\epsilon = 0.001$, $k = 50$, $\delta = 0.01$ and $\tilde{S} = 50$. As expected, due to the fact there is only one electrode and only one species takes part in the reaction, the voltammogram has a diode-like behavior: diffusion limiting in the direction of positive current and exponential growth in the direction of negative current. Also shown are the net charge densities ($\rho = c_+ - c_-$) in the double layer ($x > 0.99$) during the first cycle.

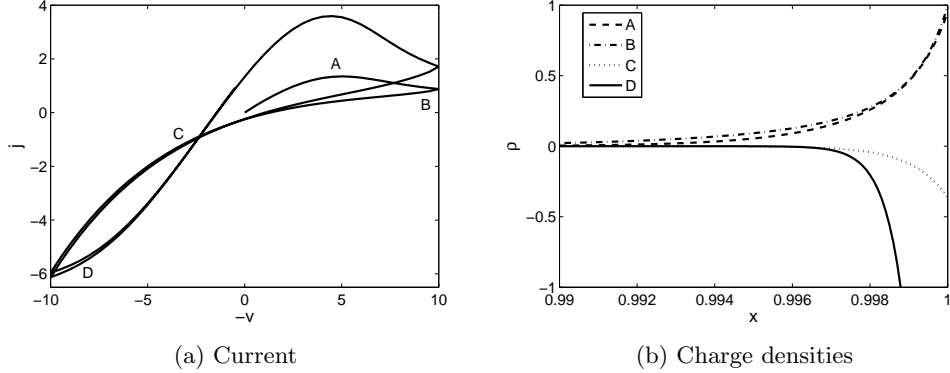


Figure 6: (a) Voltammogram for an unsupported electrolyte with one electrode subjected to a triangular voltage with $|\tilde{S}| = 50$, $\epsilon = 0.001$, $k = 50$ and $\delta = 0.01$. (b) Net charge densities $\rho = c_+ - c_-$. Labels on the charge density plot correspond to snapshots of ρ in the double layer at times labeled on the voltammogram.

5. Blocking Electrodes

5.1. Model Problem

A blocking, or ideally polarizable electrode, is one where no Faradaic reactions take place. From a modeling perspective, this means setting k_c and j_r in the Butler-Volmer equation to zero, so that current is entirely due to the displacement current term in equation (15).

Linear sweep voltammetry is a standard approach to measuring differential capacitance. In this section we consider both liquid and solid electrolytes, and both thin EDL and thick EDL (thin film) systems. Much of the early work in electrochemistry was centered around matching experimental differential capacitance curves with theory. Gouy [99] and Chapman [100] independently solved the Poisson-Boltzmann equation to obtain the differential capacitance per unit area for an electrode in a liquid electrolyte, which in the present notation can be written as

$$\tilde{C}_{\text{liquid}}(\Delta\phi) = \frac{1}{\epsilon} \cosh \frac{\Delta\phi}{2} \quad (35)$$

where $\Delta\phi$ is across the entire double layer, including the diffuse part. Later, Kornyshev and Vorotyntsev [34] performed a similar calculation for a solid electrolyte to obtain

$$\tilde{C}_{\text{solid}}(\Delta\phi) = \frac{1}{\epsilon} \frac{e^{-\Delta\phi} - 1}{\sqrt{e^{-\Delta\phi} + \Delta\phi - 1}} \text{sgn}(\Delta\phi) \quad (36)$$

Note that the capacitance for the liquid electrolyte is symmetrical about 0, but the capacitance for the solid electrolyte is not symmetrical due to the fixed charge breaking the symmetry. Also note that the displacement current in equation (15) is related to the nondimensionalized capacitance through

$$j = \frac{\epsilon^2}{2} \frac{d\phi_x}{dt} = \frac{\epsilon^2}{2} \frac{dq}{dt} = \frac{\epsilon^2}{2} \frac{dq}{dv} \frac{dv}{dt} \quad (37)$$

where $\frac{dv}{dt} = \tilde{S}$. In other words,

$$\frac{j}{\tilde{S}} = \frac{\epsilon^2}{2} \tilde{C} \sim \frac{\epsilon}{2} \quad (38)$$

and therefore ϵ is the natural scale for capacitance in our rescaled units, which we will label \tilde{C} .

In this section, we use ramp voltages to investigate the behaviour of blocking electrodes. Similar work has been done by Bazant et. al. [38], who used asymptotics to study diffuse charge effects in a system with blocking electrodes subjected to a step voltage, and Olesen et. al. [77] who used both asymptotics and simulations to do the same for sinusoidal voltages. The results of this section have applications to EDL supercapacitors [101], capacitive deionization [102, 103] and induced charge electro-osmotic (ICEO) flows [81, 104]. In the simulations in this section, δ is set to 0.01 so that we are able to have capacitance in the diffuse part of the double layer.

Both solid and liquid electrolyte systems with two blocking electrodes behave like the circuit shown in Figure 7.

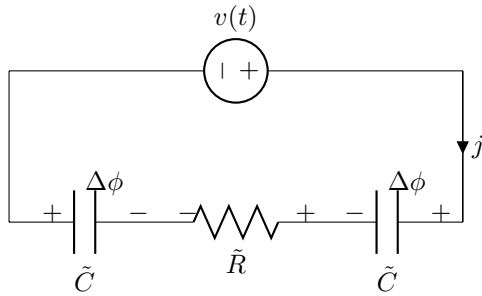


Figure 7: Equivalent circuit diagram for system with two blocking electrodes, showing the defined direction of current and polarities of the double layer capacitors. Note that \tilde{C} is a function of $\Delta\phi$.

For liquid electrolytes, $\tilde{R} \sim 2$ and for solid electrolytes, $\tilde{R} \sim 4$ [14, 12]. For liquid electrolytes, $\tilde{C}(0) = \epsilon/2$ and for solid electrolytes,

$$\tilde{C}(0) = \frac{\epsilon^2}{2} \lim_{\Delta\phi \rightarrow 0} \tilde{C}_{\text{solid}}(\Delta\phi) = \frac{\sqrt{2}\epsilon}{2} \quad (39)$$

There are two regimes of operation when a ramped voltage is applied to a capacitive system. The first is the small time ($t \ll \epsilon$) behavior, when the double layers are charged with time constant $\tau_{\text{RC}} = \tilde{R}\tilde{C}/2$, where the factor of 1/2 accounts for the fact that there are two capacitors in series. To predict the behavior during this time, we turn to the ordinary differential equation describing the circuit in Figure 7, which is

$$v(t) - 2\Delta\phi = \tilde{R}\tilde{C}(0) \frac{d\Delta\phi}{dt} \quad (40)$$

where $v(t) = \tilde{S}t$. From equation (40), the current can be solved in the case of a two

electrode liquid electrolyte to be

$$\frac{2j_{\text{inner}}(t)}{\tilde{S}} = \tilde{C}(0) \left(1 - e^{-\frac{v}{\tilde{S}\tilde{C}(0)}} \right) \quad (41)$$

where we have used $\tilde{R} = 2$ for a liquid electrolyte. The equivalent expression for solid electrolytes with single and double electrodes will be discussed in Section 5.3. Figure 8 shows a simulated plot of $\frac{2j}{SC}$ against $\frac{v}{SC}$ for a liquid electrolyte with $\epsilon = 0.001$ at early times ($t \sim \epsilon$), with a plot of $1 - e^{-x}$ for comparison. The two plots show good agreement with each other.

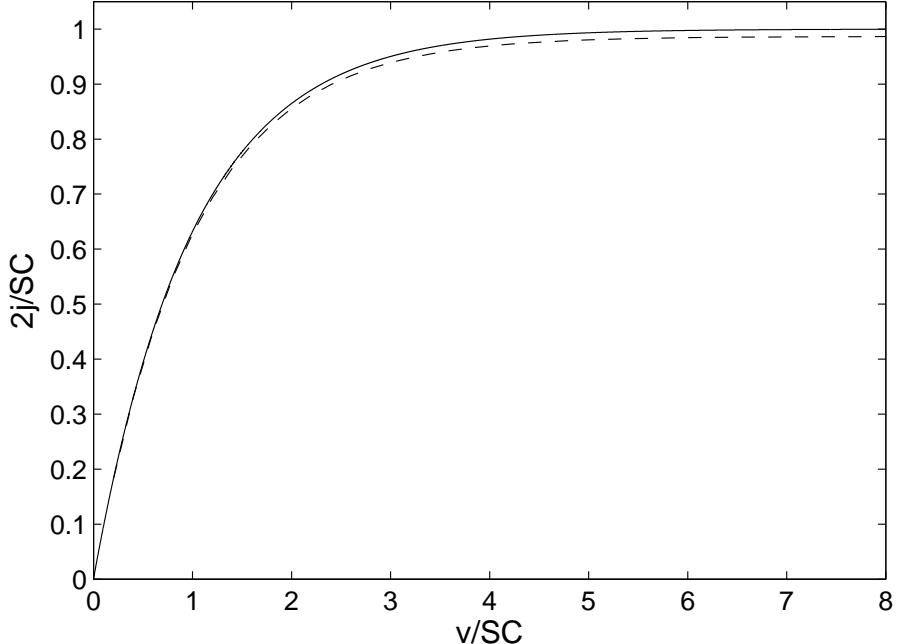


Figure 8: $\frac{2j}{SC}$ vs. $\frac{v}{SC}$ during RC charging (dashed line) and $1 - e^{-x}$ (solid line) for a liquid electrolyte with two blocking electrodes. Parameters are $\tilde{S} = -0.1$, $\epsilon = 0.001$ and $\delta = 0.01$.

The second regime of operation is the large time ($t \gg \epsilon$) behavior. After the RC charging time, the current tracks the capacitance based on equation (38). The relevant equation is

$$j = \frac{\epsilon^2}{2} \frac{dq}{dt} = \tilde{C}(\Delta\phi) \frac{d\Delta\phi}{dt} \quad (42)$$

Since we only have access to $v(t)$, the potential drop across the cell and not $\Delta\phi$, the potential drop across the double layer, we must estimate the value of $\Delta\phi$ by accounting for the resistive drop across the bulk. To do this, we can use the equation $v(t) = 2\Delta\phi + \tilde{R}j$.

In practice however, $j \ll 1$ for blocking electrodes and so we can instead just use $\Delta\phi \approx v(t)/2 = \tilde{S}t/2$. Equation (42) can then be rewritten as

$$\frac{2j_{\text{outer}}}{S} = \tilde{C}(v/2) \quad (43)$$

From equation (41) we have a solution for small times (the inner solution), and from equation (43) we have a solution for large times (the outer solution). The long time limit for the inner solution must be equal to the small time limit for the outer solution, and so the two solutions can be combined by adding them and subtracting the overlap,

$$j = j_{\text{inner}} + j_{\text{outer}} - j_{\text{overlap}} \quad (44)$$

where $2j_{\text{overlap}}/\tilde{S} = \tilde{C}(0)$, thereby creating a uniformly valid approximation of the capacitance for all values of $v(t)$.

5.2. Liquid Electrolytes

The uniformly valid approximation (equation (44)) for a liquid electrolyte with two electrodes is

$$\frac{2j}{\tilde{S}} = \tilde{C} \left(1 - e^{\frac{v}{\tilde{S}\tilde{C}}} \right) + \frac{\epsilon}{2} \cosh \frac{v}{4} - \tilde{C} \quad (45)$$

where $\tilde{C} = \epsilon/2$. Figure 9 shows $j - v$ curves for a thin EDL ($\epsilon = 0.001$) liquid electrolyte and various values of the nondimensionalized scan rate \tilde{S} .

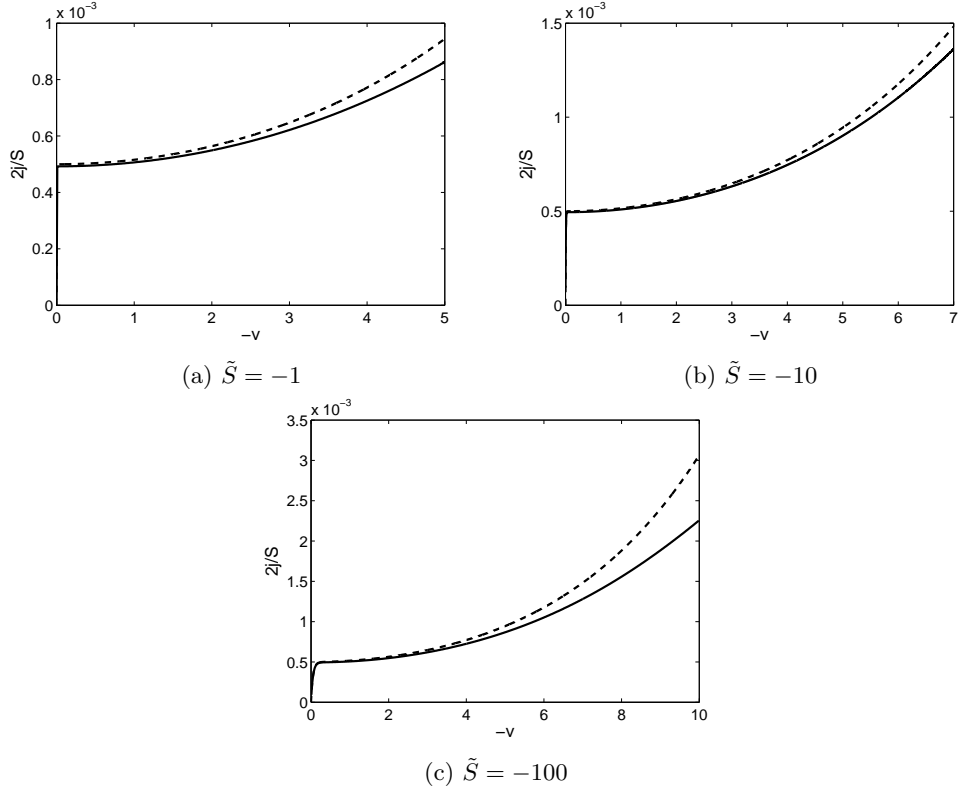


Figure 9: Simulated (solid line) and uniformly valid approximation (dashed line) j vs v curves for a thin EDL liquid electrolyte with two blocking electrodes and parameters $\epsilon = 0.001$, $\delta = 0.01$ and various values of the scan rate \tilde{S} . Solid lines are plotted from equation (45).

Next, Figure 10 shows j vs v curves for a liquid electrolyte with thick double layers ($\epsilon = 0.1$) compared to the uniformly valid approximation, equation (45). At higher voltages in liquid electrolytes with thick double layers, the two double layers begin to overlap, and then nearly all of the concentration migrates to one electrode. This can be seen in Figure 11, which shows cation concentration at various points during the $\tilde{S} = 0.1$ sweep. This results in the depression of the capacitance at high voltages seen in Figure 10.

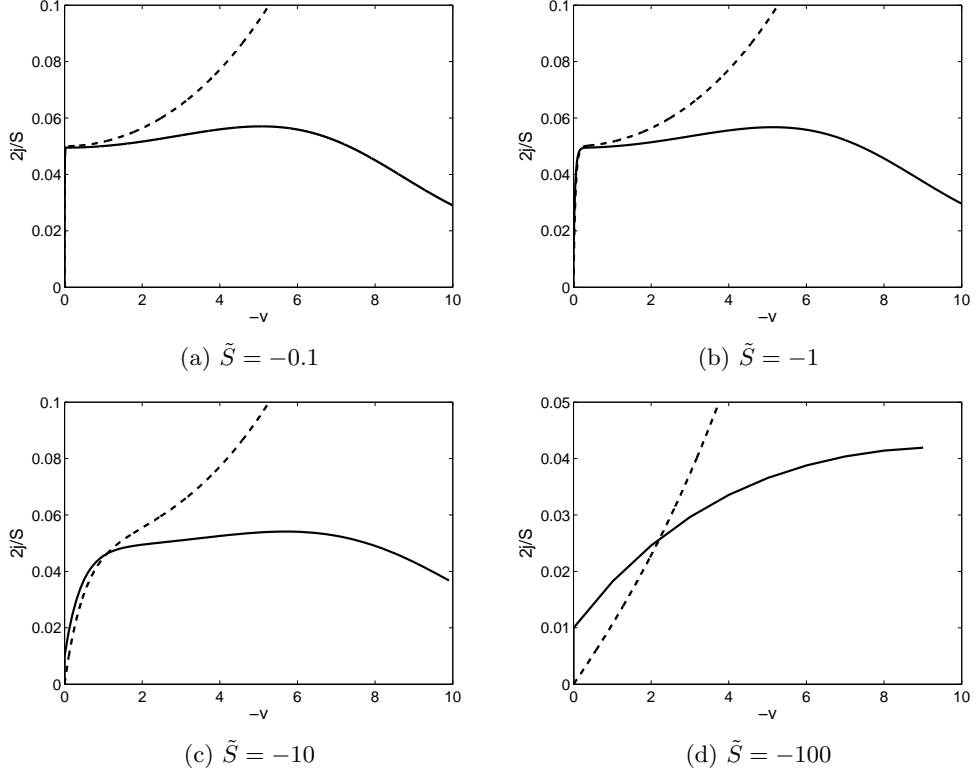


Figure 10: Simulated (solid line) and uniformly valid approximation (dashed line) j vs v curves for a thick EDL liquid electrolyte with two blocking electrodes and parameters $\epsilon = 0.1$, $\delta = 0.01$ and various values of \tilde{S} . Solid lines are plotted from equation (45).

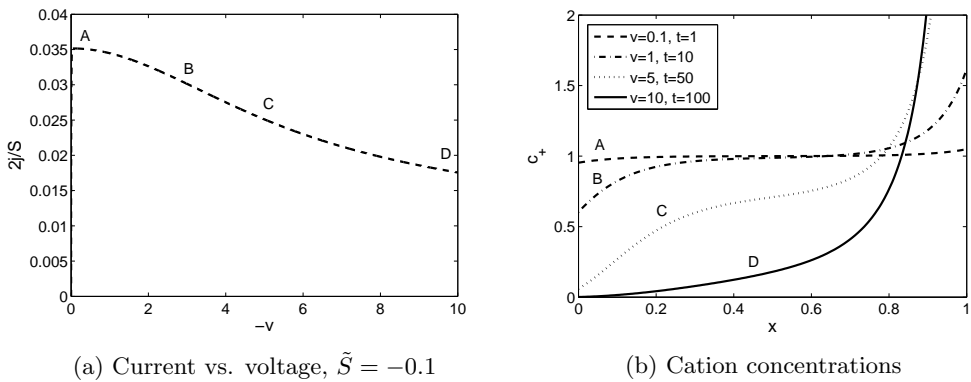


Figure 11: (a) j vs. v and (b) cation concentrations for a thick EDL liquid electrolyte with two blocking electrodes and parameters $\epsilon = 0.1$, $\delta = 0.01$ and scan rate $\tilde{S} = -0.1$. Labels in (a) correspond to cation concentrations in (b) at various times.

5.3. Solid Electrolytes

Since the capacitance for a solid electrolyte (equation (36)) is not symmetrical about $\Delta\phi = 0$, the capacitance for a solid electrolyte system with two blocking electrodes can be represented by the two capacitors in series,

$$\frac{1}{\tilde{C}_{\text{solid}}(\Delta\phi)} = \frac{1}{\tilde{C}_{\text{solid}}(\Delta\phi)} + \frac{1}{\tilde{C}_{\text{solid}}(-\Delta\phi)} \quad (46)$$

The uniformly valid approximation for a solid electrolyte with one electrode is

$$\frac{j}{\tilde{S}} = \tilde{C} \left(1 - e^{\frac{v}{2\tilde{C}}} \right) + \epsilon \frac{e^{-v} - 1}{\sqrt{e^{-v} + v - 1}} \text{sgn}(v) - \tilde{C} \quad (47)$$

where $\tilde{C} = \sqrt{2\epsilon}$. Using equation (46), the approximation for two electrodes is

$$\frac{2j}{\tilde{S}} = \tilde{C} \left(1 - e^{\frac{v}{2\tilde{S}\tilde{C}}} \right) + \frac{\epsilon}{2} \left(\frac{e^{-\frac{v}{2}} - 1}{\sqrt{e^{-\frac{v}{2}} + \frac{v}{2} - 1}} \text{sgn}(v) \parallel \frac{e^{\frac{v}{2}} - 1}{\sqrt{e^{\frac{v}{2}} - \frac{v}{2} - 1}} \text{sgn}(-v) \right) - \tilde{C} \quad (48)$$

where $\tilde{C} = \frac{\epsilon}{2\sqrt{2}}$ and \parallel indicates the reciprocal of the sum of the reciprocals (the parallel circuit symbol), i.e. $A \parallel B = 1/(1/A + 1/B)$. The additional factor of 1/2 in the exponent in the inner part of equation (48) is due to the fact that the electrolyte resistance for solid electrolytes is 4 rather than 2.

Figure 12 shows the j vs v curve for $\tilde{S} = 1$ compared to the theoretical result for a thin EDL solid electrolyte with a single electrode, and sees good agreement between the simulated results and our approximation from equation (47).

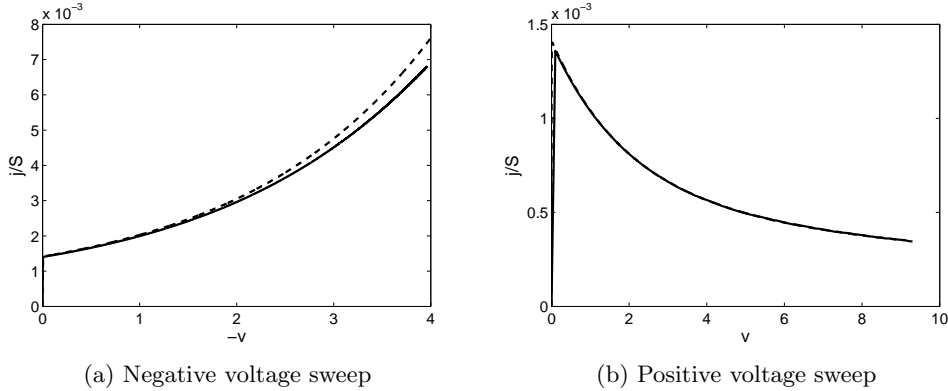


Figure 12: Simulated (solid line) vs. uniformly valid approximation (dashed line) j vs v curves for a thin EDL solid electrolyte with a single blocking electrode and parameters $\epsilon = 0.001$, $\delta = 0.01$ and $\tilde{S} = \pm 1$. Figure (a) shows the negative part of the sweep and Figure (b) shows the positive part. Solid lines are plotted from equation (47).

Next, Figure 13 shows j vs v curves for a thin EDL ($\epsilon = 0.001$) solid electrolyte with two blocking electrodes for various values of \tilde{S} , compared to the uniformly valid approximation from equation (48).

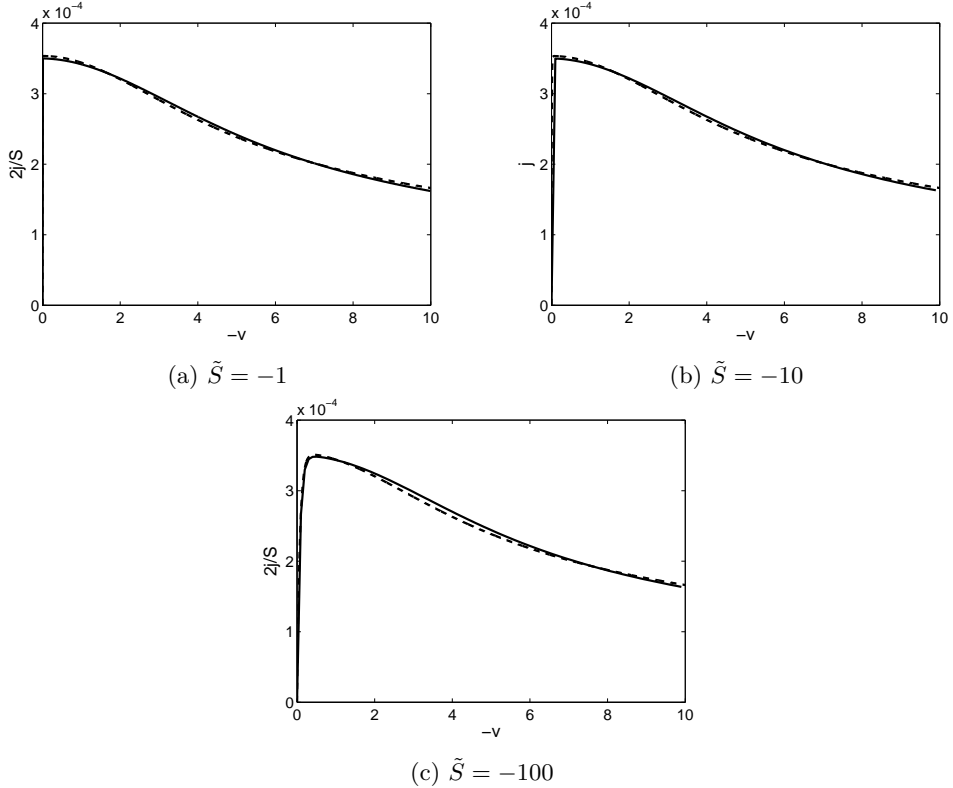


Figure 13: Simulated (solid line) and uniformly valid approximation (dashed line) j vs v curves for a thin EDL solid electrolyte with two blocking electrodes and parameters $\epsilon = 0.001$, $\delta = 0.01$ for various values of \tilde{S} . Solid lines are plotted from equation (48).

Finally, Figures 14 and 15 show the single and double electrode responses for a thick EDL ($\epsilon = 0.1$) solid electrolyte.

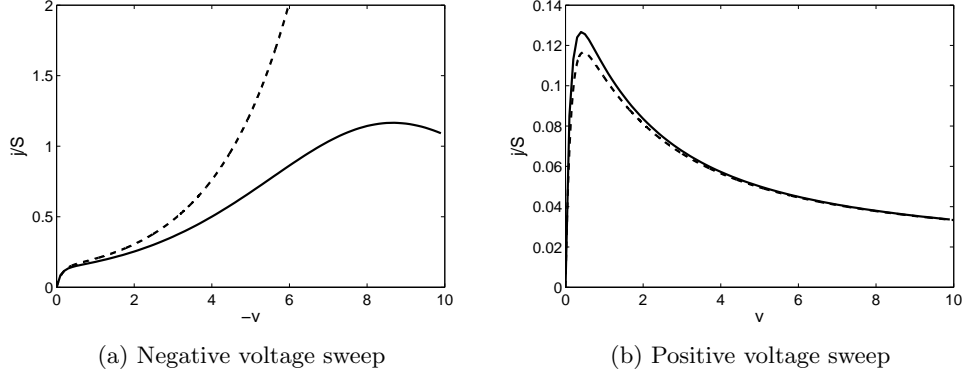


Figure 14: Simulated (solid line) and uniformly valid approximation (dashed line) j vs v curves for a thick EDL solid electrolyte with a single blocking electrode and parameters $\epsilon = 0.1$, $\delta = 0.01$ and $\tilde{S} = \pm 1$. Figure (a) shows the negative voltage sweep and Figure (b) shows the positive voltage sweep. Solid lines are plotted from equation (47).

The disagreement between our simulations and the uniformly valid approximation in Figure 14a may be due to current limiting, since the simulation uses $\tilde{S} = 1$ so $j/\tilde{S} = j$, which has a classical limiting current of 1. The double electrode results in Figure 15 show generally good agreement with theory.

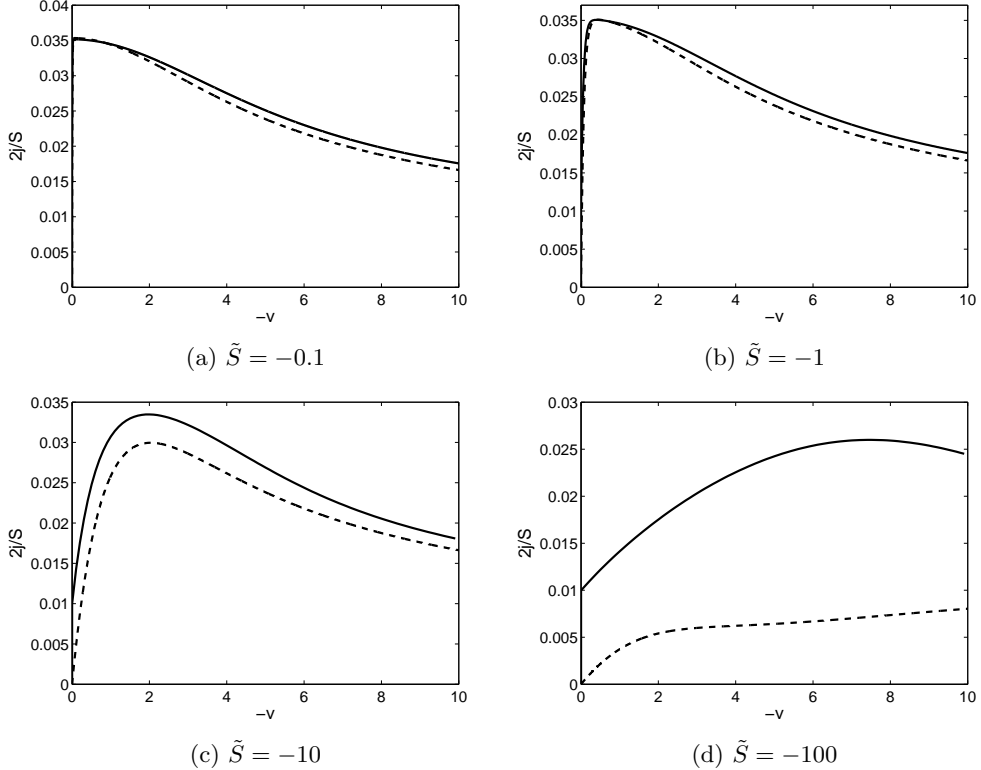


Figure 15: Simulated (solid line) and uniformly valid approximation (dashed line) j vs. v curves for a thick EDL solid electrolyte with two blocking electrodes and parameters $\epsilon = 0.1$, $\delta = 0.01$ and various values of \tilde{S} . Solid lines are plotted from equation (48)

6. Liquid Electrolyte Thin Films

6.1. Model Problem

In this section, we study voltammograms of liquid electrolyte electrochemical thin films. General steady-state models for thin films have been previously presented in [12] and [13] as well as in [14], with a time-dependent model considered in [49]. In the present work, we consider voltage ramps on systems with two dissimilar electrodes, i.e. values of k_c and j_r such that an equilibrium voltage develops across the cell.

6.2. Low Sweep Rates

6.2.1. Thin EDL

At low sweep rates, the current-voltage relationship approaches the steady-state response, which for solid and liquid electrolytes was derived by Bazant et al. [12] (for an electrolytic cell with two identical electrodes) and Biesheuvel et al. [14] (for a galvanic

cell with two different electrodes). For a liquid electrolyte, the cell voltage is given in the GC ($\delta \rightarrow 0$) limit by

$$v(j) = v_0 - 4 \operatorname{arctanh}(j) + \ln \frac{1 - j/j_{r,A}}{1 + j/j_{r,C}} \quad (49)$$

and in the H limit ($\delta \rightarrow \infty$) by

$$v(j) = v_0 - 4 \operatorname{arctanh}(j) - 2 \operatorname{arcsinh} \frac{j}{\sqrt{\beta_A(1+j)}} - 2 \operatorname{arcsinh} \frac{j}{\sqrt{\beta_C(1-j)}} \quad (50)$$

where $v_0 = \ln \frac{k_{c,C} j_{r,A}}{k_{c,A} j_{r,C}}$ is the equilibrium voltage, $\beta_A = 4k_{c,A} j_{r,A}$ and $\beta_C = 4k_{c,C} j_{r,C}$. The subscripts A and C denote parameter values at the anode and cathode, respectively.

Figure 16 shows v vs j curves for a solid electrolyte for $k_{c,C} = 30$, $k_{c,A} = 1$, $j_{r,C} = 0.1$, $j_{r,A} = 0.8$ (the same as Figure 3 in [14]) for an open circuit voltage of $v_0 \approx 5.5$ and various values of δ along with the GC and H limits from equations (49)–(50). The curves were created with a voltage ramp from -10 to $+15$ with a scan rate of $\tilde{S} = 2.5$. The $\delta = 1$ and $\delta = 10$ curves were generated with $\epsilon = 0.001$, while the $\delta = 0.1$ and $\delta = 0.01$ curves with $\epsilon = 0.005$.

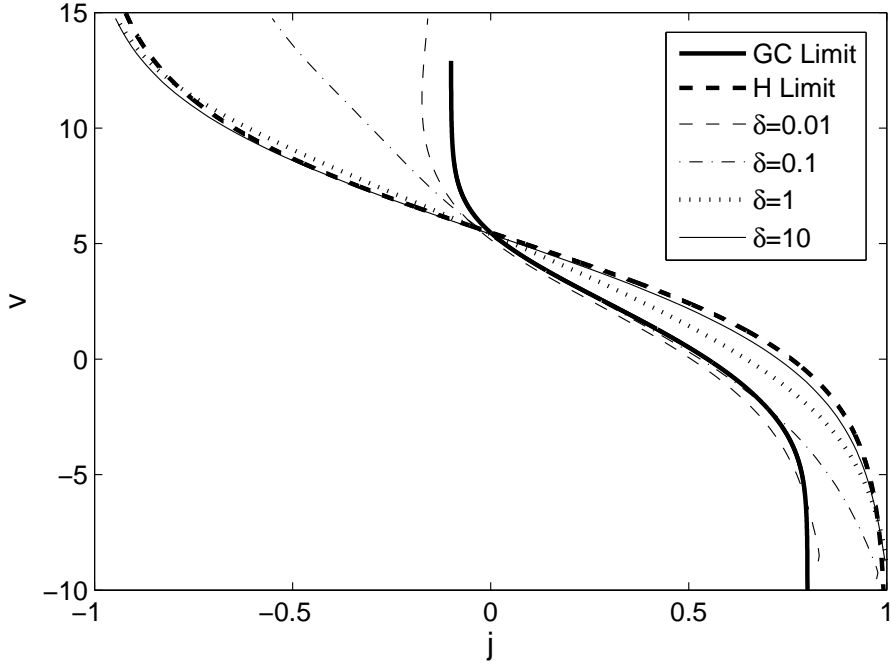


Figure 16: v vs j curves for a thin EDL liquid electrolyte with two electrodes and with parameters $\epsilon = 0.001$ ($\delta = 1, 10$) and $\epsilon = 0.005$ ($\delta = 0.1, 0.01$), $k_{c,C} = 30$, $k_{c,A} = 1$, $j_{r,C} = 0.1$ and $j_{r,A} = 0.8$ ($v_0 \approx 5.5$). Also shown are the steady-state curves in the GC and H limits from equations (49) and (50), respectively. Simulated curves were created using a voltage scan rate of $\tilde{S} = 2.5$.

As expected, the voltage-current response for a liquid electrolyte is seen in Figure 16 to have reaction limits at $j = -j_{r,C} = -0.1$ and $j = j_{r,A} = 0.8$ in the GC limit, and diffusion limits at $j = \pm 1$ in the H limit. The limiting cases from equations (49)–(50) also do not strictly bound the simulated results in Figure 16 due to the non-monotonic dependence of the cell voltage $\Delta\phi$ on δ [14].

6.2.2. Thick EDL

Figure 17 shows j vs v for a thick EDL liquid electrolyte with two electrodes, with various values of $k_{c,C}$. $\epsilon = 0.1$, $\delta = 1$, scan rate $\tilde{S} = 2.5$, with other reaction rate parameters the same as in Figure 16. Since the voltage sweep rate is slow compared to both reaction and diffusion and ϵ is large enough that the double layers are able to overlap and interact with each other, the current vs. voltage curve straightens out compared to a thin double layer system, becoming effectively ohmic in nature.

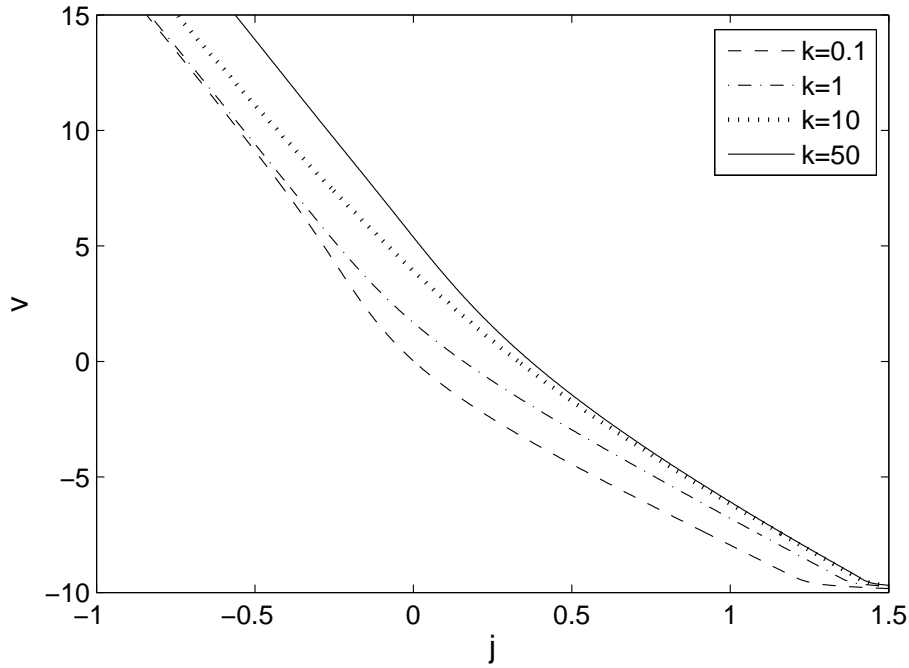


Figure 17: j vs v for a thick EDL liquid electrolyte with two electrodes, with various values of $k_{c,C}$. $\epsilon = 0.1$, $\delta = 1$, scan rate $\tilde{S} = 2.5$ and other reaction rate parameters the same as in Figure 16.

6.3. Diffusion versus Reaction Limitation

When sweep rates are fast, current-voltage curves will differ from the slow sweep results in Section 6.2 due to physical limitation of the speed at which current can be produced at electrodes. This nonlinear interdependence of current and voltage when current flows into an electrode is referred to in electrochemistry by the blanket term

polarization, not to be confused with the dielectric polarization. Generally speaking, when current flows across a cell, its cell potential, v , will change. The difference between the equilibrium value of v and its value when current is applied is commonly referred to as the *overpotential* or *overvoltage* and labeled η .

Very briefly, there are three competing sources of overpotential in an electrochemical cell:

1. Ohmic polarization is caused by the slowness of electromigration in the bulk. When a cell behaves primarily ohmically, it is characterized by a linear j - v curve which can be written as $\eta_{\text{ohm}} = r_{\text{cell}}j$. When this behavior is modeled by a circuit, it is usually represented as a single resistor between the two electrodes.
2. Kinetic polarization is due to the slowness of electrode reactions (k small). Using the overpotential version of the Butler-Volmer equation as a starting point, and assuming fast transport of species to and from the electrode ($C_{\text{electrode}} = C_{\text{bulk}}$), we can invert the equation to find

$$\eta_{\text{kin}} = \text{arcsinh} \left(\frac{j}{j_0} \right) \quad (51)$$

where j_0 is the nondimensional exchange current density. Thus, when kinetic polarization is the primary cause of overpotential, the j - v curve takes on an exponential characteristic. This type of polarization is represented by a charge-transfer resistance in circuit models.

3. Transport, or concentration polarization is due to slowness in the supply of reactants or removal of products from the electrode, resulting in a depletion of reactants at the electrode. Concentration polarization is characterized by a saturation of the current-voltage relationship, and is represented by the frequency-dependent Warburg element in circuit models.

Figure 18 shows the current vs. voltage characteristic for a two-electrode cell with fast reactions ($k = 50$) and \tilde{S} varied. When \tilde{S} is large, diffusion limitation sets in and the current can be seen to approach saturation. When \tilde{S} is small, the relationship is ohmic, i.e. linear response. For plots where the sweep rate \tilde{S} varies, we only plot the Faradaic part of the current (the second term on the right hand side of equation (15)) since for $\tilde{S} \gg 1$ there is a significant displacement component.

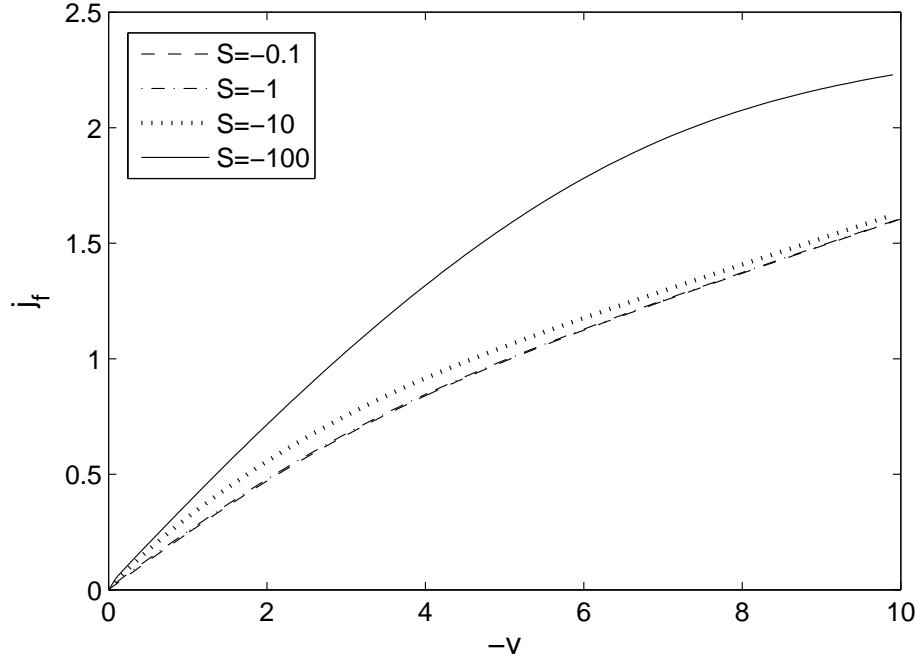


Figure 18: Faradaic current vs. voltage for a liquid electrolyte with two electrodes with \tilde{S} varied and with parameters $\epsilon = 0.05$, $\delta = 1$ and $k_{c,a} = 50 = j_{r,a} = k_{c,c} = j_{r,c} = 50$ ($v_0 = 0$). Diffusion limitation is seen to set in at higher voltages in the $\tilde{S} = -100$ plot.

Figure 19 shows Faradaic current vs voltage for a liquid electrolyte with two electrodes and with \tilde{S} varied and parameters $\epsilon = 0.05$, $\delta = 1$, $k_{c,a} = 50$, $j_{r,a} = 100$, $k_{c,c} = 0.1$, and $j_{r,c} = 0.05$ ($v_0 \approx 1.4$). As \tilde{S} increases, the j - v curve is seen to take on a more pronounced exponential character, thus showing the effect of reaction limitation.

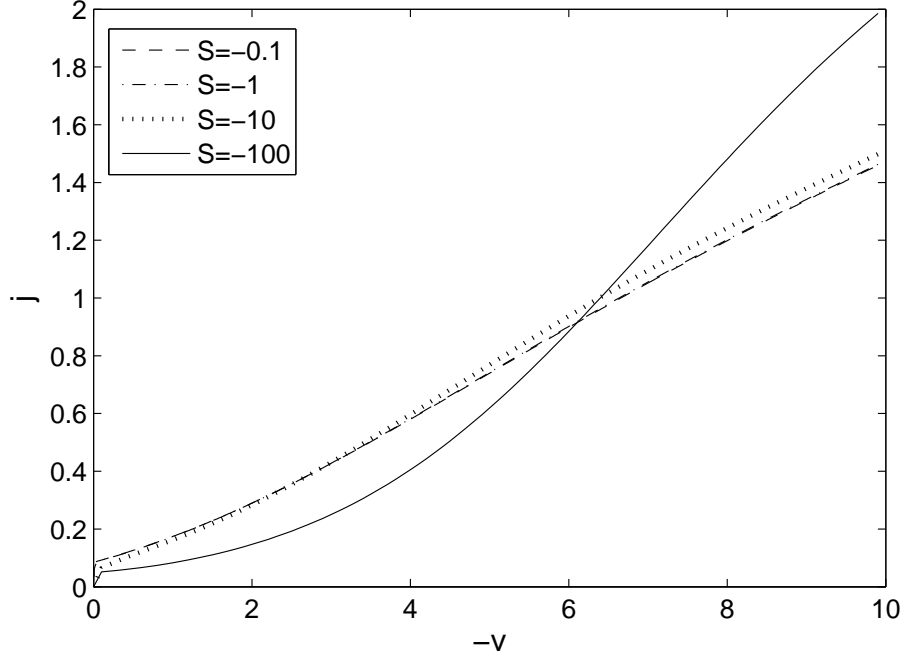


Figure 19: Faradaic current vs. voltage for a liquid electrolyte with two electrodes and with \tilde{S} varied, with parameters $\epsilon = 0.05$, $\delta = 1$, $k_{c,a} = 50$, $j_{r,a} = 100$, $k_{c,c} = 0.1$ and $j_{r,c} = 0.05$ ($v_0 \approx 1.4$). A current response dominated by reaction limitation is seen in the $\tilde{S} = -100$ plot.

6.4. Transient Space Charge

The development of a space charge region, or a region of net charge outside of the double layer where $\rho = c_+ - c_- \neq 0$, is a strongly nonlinear effect that was predicted by Bazant, Thornton & Ajdari [38] and solved by Olesen, Bazant & Bruus using asymptotics and simulations for large sinusoidal voltages [77]. Figure 20 shows the voltammogram of a system subjected to a triangular voltage with $\epsilon = 0.001$, $\delta = 0.3$, $k = 50$ and $\tilde{S} = 100$, and Figure 21 shows the development of space charge regions.

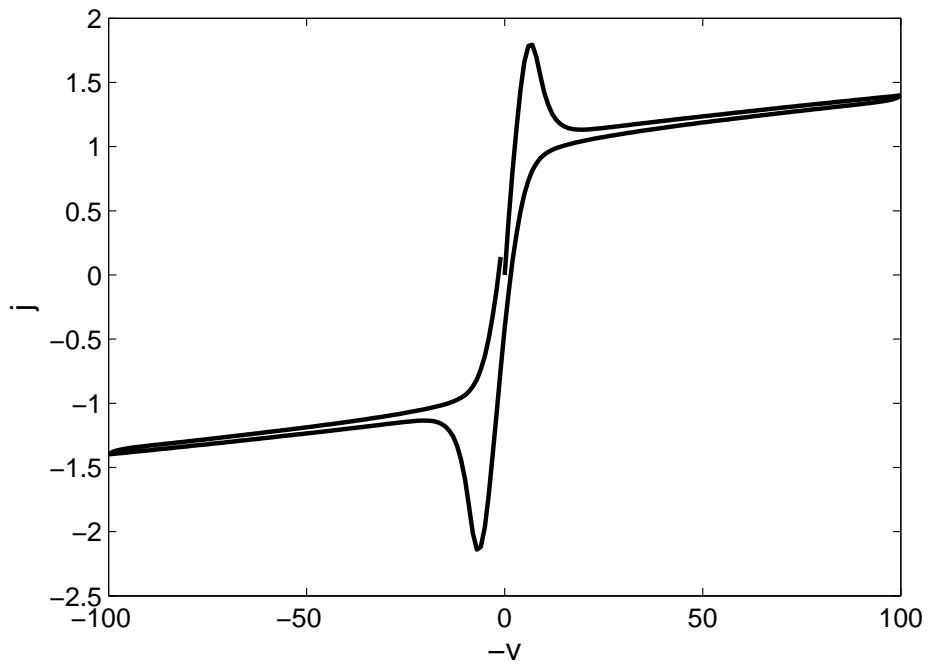


Figure 20: Voltammogram for a thin EDL liquid electrolyte with two electrodes subjected to a triangular voltage with $\epsilon = 0.001$, $\delta = 0.3$, $k = 50$ and $|\tilde{S}| = 100$. Concentrations with development of space charge regions are shown in Figure 21.

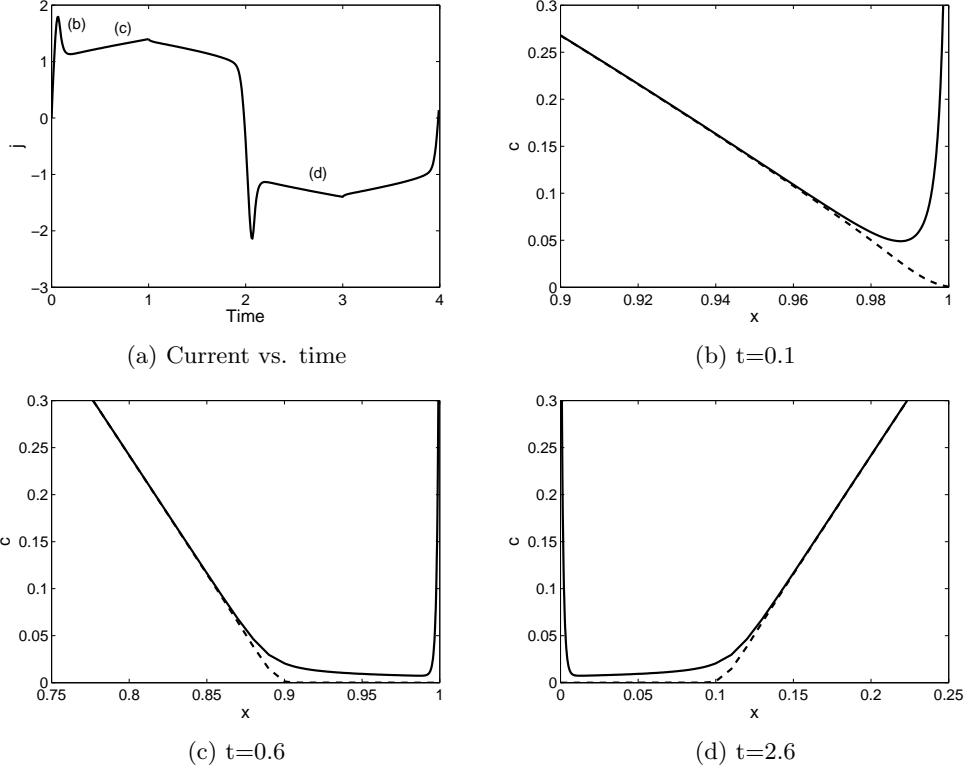


Figure 21: (a) Current and (b-d) resulting cation (solid line) and anion (dashed line) concentrations showing space charge regions developed at the cathode and anode from a triangular applied voltage in a thin EDL liquid electrolyte with two electrodes. Parameters used were $\epsilon = 0.001$, $\delta = 0.3$, $k = 50$, and $|\tilde{S}| = 100$.

The current-voltage response during space charge formation is a transient case of a diffusion limited system ($\tilde{S}, k \gg 1$) being driven above the limiting current [13, 24, 88] and the subsequent breakdown of electroneutrality in the bulk. Figure 21 shows the current peaking as diffusion limiting sets in ($t = 0.1$) and anion concentration at the cathode reaches zero (Figure 21b). After this time, a space charge region begins to form outside of the double layer as seen in Figure 21c, and the current ramps up slowly until the voltage reverses direction. Since the cell is symmetrical, the same thing occurs at the anode during the positive voltage part of the cycle, with current flowing in the other direction (Figure 21d). The height of the current peak and slope of current during space charge development are dependent on the value of \tilde{S} .

An effect which is not included in the simulation that could prove important is ionic crowding [105], as both concentrations reach large values (i.e. $c_-(x = 0, t = 0.6) \approx 4$) at the electrodes. It may be interesting to extend these simulations to include steric effects in future work.

7. Solid Electrolyte Thin Films

7.1. Model Problem

In this section, we consider ramp voltages applied to solid electrolyte electrochemical thin films. The counterion concentration is fixed, i.e.

$$c_-(x, t) = 1 \quad (52)$$

7.2. Low Sweep Rates

7.2.1. Thin EDL

For a solid electrolyte in the thin EDL limit, the cell voltage is given in the GC limit by

$$v(j) = v_0 - 4j + \ln \frac{1 - j/j_{r,A}}{1 + j/j_{r,C}} \quad (53)$$

and in the H limit by

$$v(j) = v_0 - 4j - 2 \operatorname{arcsinh} \frac{j}{\sqrt{\beta_A}} - 2 \operatorname{arcsinh} \frac{j}{\sqrt{\beta_C}} \quad (54)$$

Figure 22 shows v vs j curves for a solid electrolyte for $\epsilon = 0.001$, $k_{c,C} = 30$, $k_{c,A} = 1$, $j_{r,C} = 0.1$, $j_{r,A} = 0.8$ (the same as [14] Figure 3) and various values of δ along with the GC and H limits from equations (53)–(54). The curves were created with a voltage ramp from -10 to +15 and with a scan rate of $\tilde{S} = 2.5$.

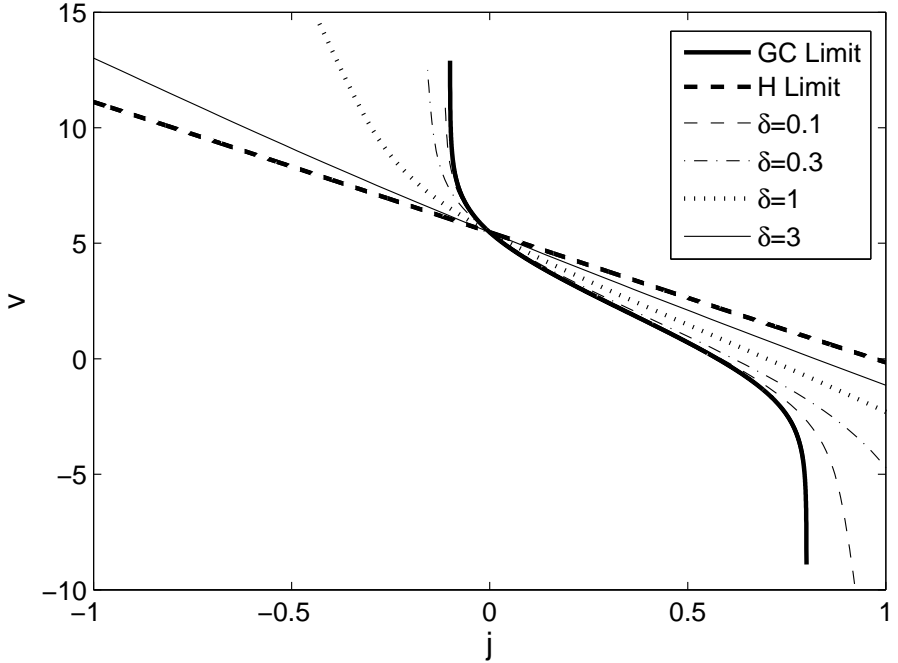


Figure 22: v vs j curves for a thin EDL solid electrolyte with two electrodes and with $\epsilon = 0.001$, $k_{c,C} = 30$, $k_{c,A} = 1$, $j_{r,C} = 0.1$, $j_{r,A} = 0.8$ ($v_0 \approx 5.5$) and δ varied. Also shown are the steady-state curves in the GC and H limits from equations (53) and (54), respectively. Simulated curves were created using a voltage scan rate of $\tilde{S} = 2.5$.

Compared to the liquid electrolyte case, the two limits on δ for fixed countercharge are seen in Figure 22 to have a reaction limits at $j = -j_{r,C} = -0.2$ and $j = j_{r,A} = 0.8$ in the GC limit, but no diffusion limit in the H limit, which is consistent with the expected behavior for a solid electrolyte.

7.2.2. Thick EDL

Figure 23 shows j vs v for a thick EDL solid electrolyte with two electrodes, with various values of $k_{c,C}$. $\epsilon = 0.1$, $\delta = 1$, scan rate $\tilde{S} = 2.5$, with other reaction rate parameters the same as in Figure 22. As in the liquid case, the sweep rate is too slow for any polarization effects to occur, and the current response remains ohmic over the voltage range.

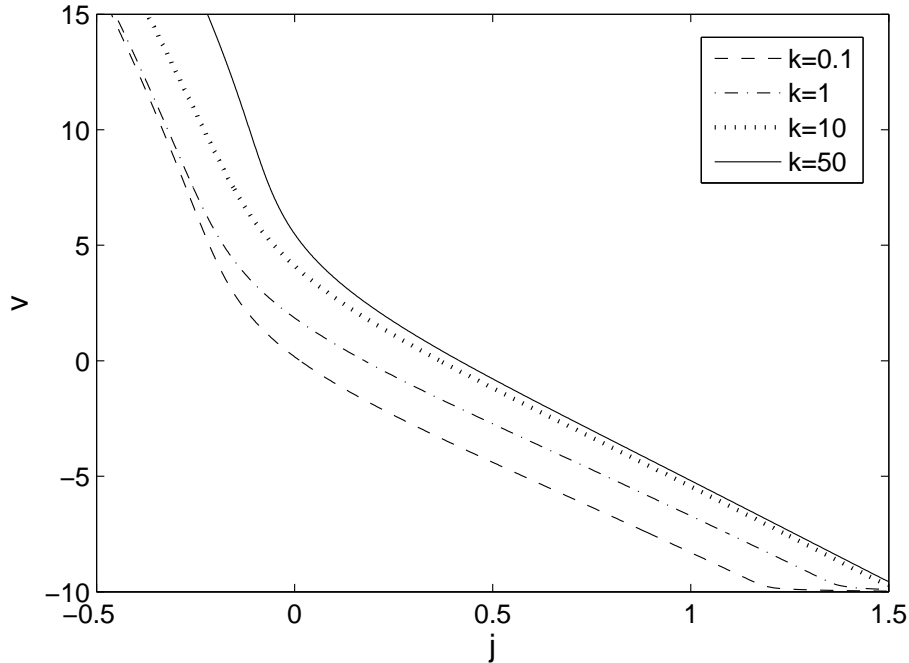


Figure 23: j vs v for a thick EDL solid electrolyte with two electrodes, with various values of $k_{c,C}$. $\epsilon = 0.1$, $\delta = 1$, scan rate $\tilde{S} = 2.5$ and other reaction rate parameters the same as in Figure 22.

7.3. Diffusion versus Reaction Limitation

In terms of electrode polarization, the key difference between liquid and solid electrolytes is that the imposed constant counterion concentration associated with a solid electrolyte does not allow diffusion limiting to occur, since the reacting species is not allowed to be depleted at the electrodes. This can be seen in Figure 24, where the current remains linear with respect to voltage even at high sweep rates.

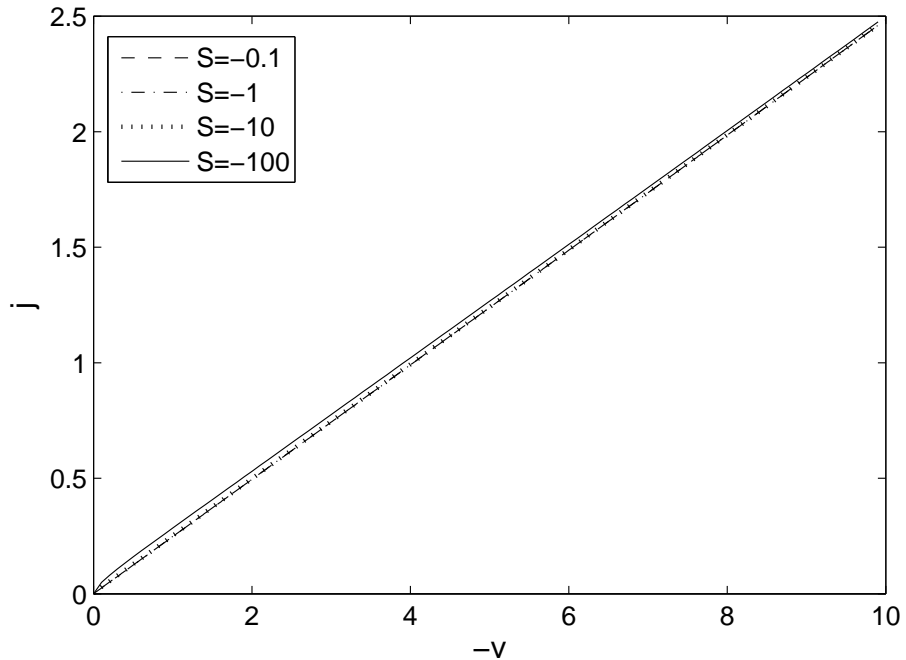


Figure 24: Faradaic current vs. voltage for a solid electrolyte with two electrodes with \tilde{S} varied and with parameters $\epsilon = 0.05$, $\delta = 1$ and $k_{c,a} = 50 = j_{r,a} = k_{c,c} = j_{r,c} = 50$ ($v_0 = 0$). No diffusion limitation is allowed in solid electrolytes, and so the j vs. v curves are linear for all values of \tilde{S} .

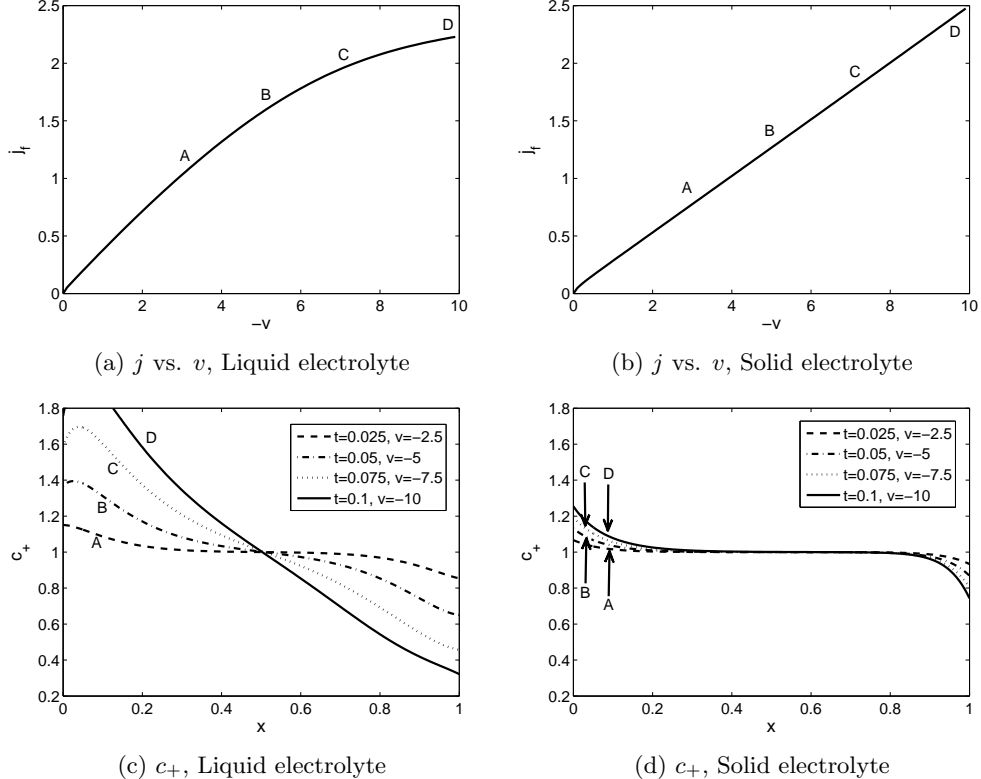


Figure 25: (a), (b) j vs. v and (c), (d) cation concentrations c_+ at $t = 0.025$ (dashed line), 0.05 (dash-dotted line), 0.075 (dotted line) and 0.1 (solid line) for $\tilde{S} = -100$ voltage sweeps on both liquid and solid electrolytes with two electrodes. Other parameters are the same as in Figures 18 and 24.

Figure 26 shows the current vs voltage curve for a solid electrolyte with \tilde{S} varied. $\epsilon = 0.05$, $\delta = 1$, $k_{c,a} = 50$, $j_{r,a} = 100$, $k_{c,c} = 0.1$, $j_{r,a} = 0.05$ ($v_0 \approx 1.4$). As in the liquid electrolyte case, high sweep rates cause the system to become primarily reaction-limited, producing an exponential curve. At lower \tilde{S} , the response remains ohmic, and so the curves approach a straight line.

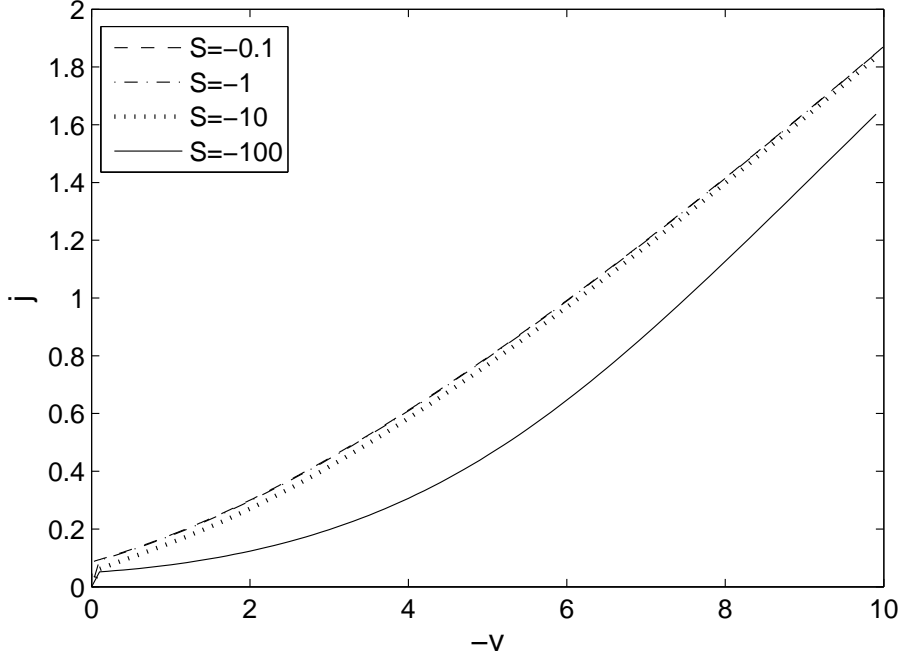


Figure 26: Faradaic current vs. voltage for a solid electrolyte with two electrodes and with \tilde{S} varied, with parameters $\epsilon = 0.05$, $\delta = 1$, $k_{c,a} = 50$, $j_{r,a} = 100$, $k_{c,c} = 0.1$ and $j_{r,c} = 0.05$ ($v_0 \approx 1.4$). Reaction limitation is prominent in the $\tilde{S} = -100$ curve.

8. Leaky Membranes

8.1. Model Problem

Finally, we consider the classical description of membranes as having constant, uniform background charge density ρ_s , in addition to the mobile ions [106, 107, 108, 109]. In this section, we focus on the strongly nonlinear regime of small background charge and large currents in a “leaky membrane” [28, 110]. This situation can arise as a simple description of micro/nanochannels with charged surfaces, as well as traditional porous media, neglecting electro-osmotic flows. For example, Figure 27 shows a representation of a microchannel with negative charge on its side walls, where surface conduction through the positively charged diffuse double layers can sustain over-limiting current (faster than diffusion) [27] and deionization shock waves [111]. This phenomenon has applications to desalination by shock electrodialysis [29, 30], as well as metal growth by shock electrodeposition [31, 32], and the following analysis could be used to interpret LSV for such electrochemical systems with bulk fixed charge.

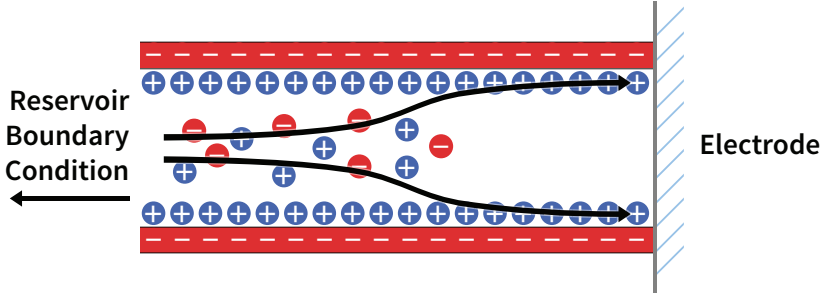


Figure 27: Surface conduction in a microchannel with negative wall charge. Black arrow represents the direction of current. Positive ions in the electrolyte screens the wall charge, resulting in a negative excess background charge in the electrolyte. Overlimiting current is able to occur due to surface conduction past the depletion caused by concentration polarization.

The appropriate modification to the Poisson equation for a background charge is

$$-\varepsilon_s \frac{\partial^2 \Phi}{\partial X^2} = F (C_+ - C_- + \rho_s) \quad (55)$$

Equation (55) is nondimensionalized to

$$-2\epsilon^2 \frac{\partial^2 \phi}{\partial x^2} = z_+ c_+ + z_- c_- + 2\tilde{\rho}_s \quad (56)$$

where $\tilde{\rho}_s = \rho_s/(2C_0F)$. Equations (55)–(56) are equivalent to the “uniform potential model” and “fine capillary model” [112] and have a long history in membrane science cite-Teorell1935, Meyer1936, Spiegler1971.

The time-independent equations for the bulk charged electrolyte without electrode interfaces can be solved to obtain the steady-state current-voltage relationship [27], which is given by

$$j = \frac{1 - e^{-|v|/2} - \tilde{\rho}_s|v|}{2} \quad (57)$$

where the factor of one half is due to a difference in our definition of the scaling current (in equation (15)) from [27]. This expression has been successfully fitted to quasi-steady current voltage relations in experiments [29, 31, 32], which in fact were obtained by LSV at low sweep rates, so it is important to understand the effects of finite sweep rates. In Sections 8.2–8.3, we present simulation results for ramped and cyclic voltammetry on systems with negative and positive background charge.

8.2. Negative Background Charge

First, we consider the case where the sign of the background charge is opposite to that of the reactive cations, which avoid depletion by screening the fixed background charge. This is the most interesting case for applications of leaky membranes [29, 30, 31, 32], since the system can sustain over-limiting current. Figure 28 shows current in response to voltage ramps with $\epsilon = 0.005$, $\delta = 10$, $\rho_s = -0.01$ and $k = 50$, with various values

for \tilde{S} . The limiting behavior for the current for small \tilde{S} can be predicted by the steady state response from equation (57). As observed in multiple experiments [29, 31, 32], a bump of current overshoot occurs prior to steady state for high sweep rates, which we can attribute to diffusion limitation during transient concentration polarization in the leaky membrane. Similar bumps have also been predicted by Moya et al. [94] for neutral electrolytes in contact with (non-leaky) ion-exchange membranes with quasi-equilibrium double layers.

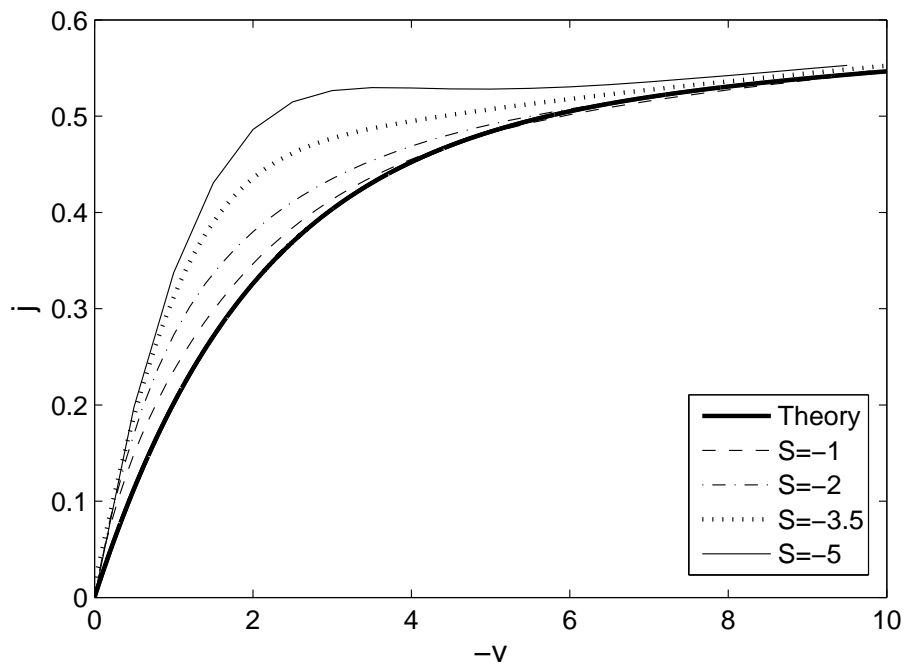


Figure 28: Current in response to a voltage ramp in a liquid electrolyte with one electrode and constant background charge. Parameters are $\epsilon = 0.005$, $\delta = 10$, $\rho_s = -0.01$ and $k = 50$. Also shown is the steady state response from equation (57).

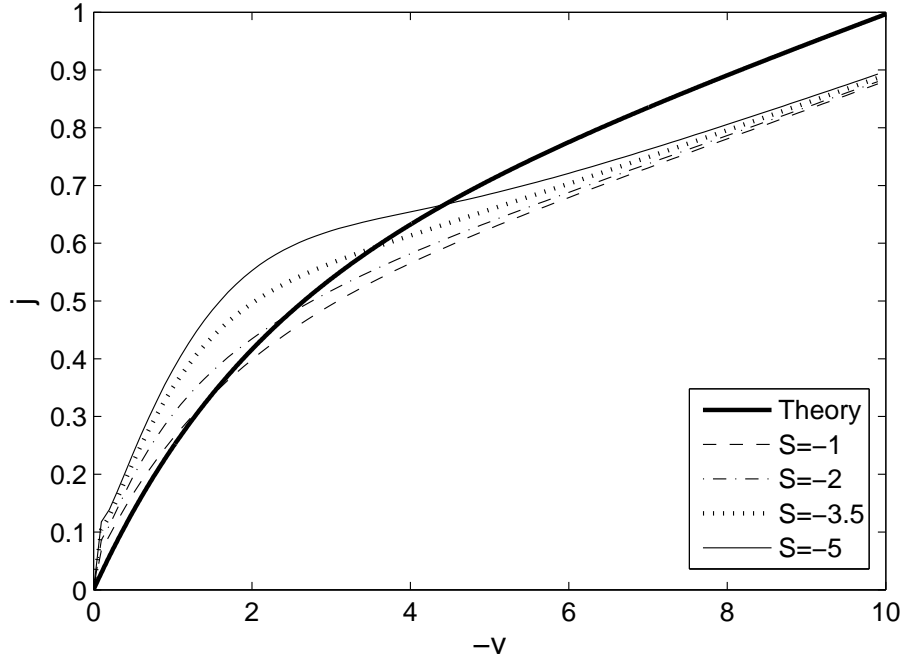


Figure 29: Current from a voltage ramp applied to a liquid electrolyte with a single electrode and constant background charge. Parameters are $\epsilon = 0.005$, $\delta = 10$, $\rho_s = -0.1$ and $k = 50$. Also shown is the steady state response from equation (57).

Next, Figures 30 and 31 show cyclic voltammograms and corresponding concentration profiles for background charges of $\rho_s = -0.01$ and $\rho_s = -0.1$, respectively, with $\tilde{S} = 10$. Due to the additional background charge, the concentrations in the bulk are slightly different. For a 1:1 electrolyte, this difference is exactly $-2\rho_s$, as in equation (56). For an electrolyte that is not 1:1, the difference can be obtained using $z_+c_+ + z_-c_- = -2\rho_s$.

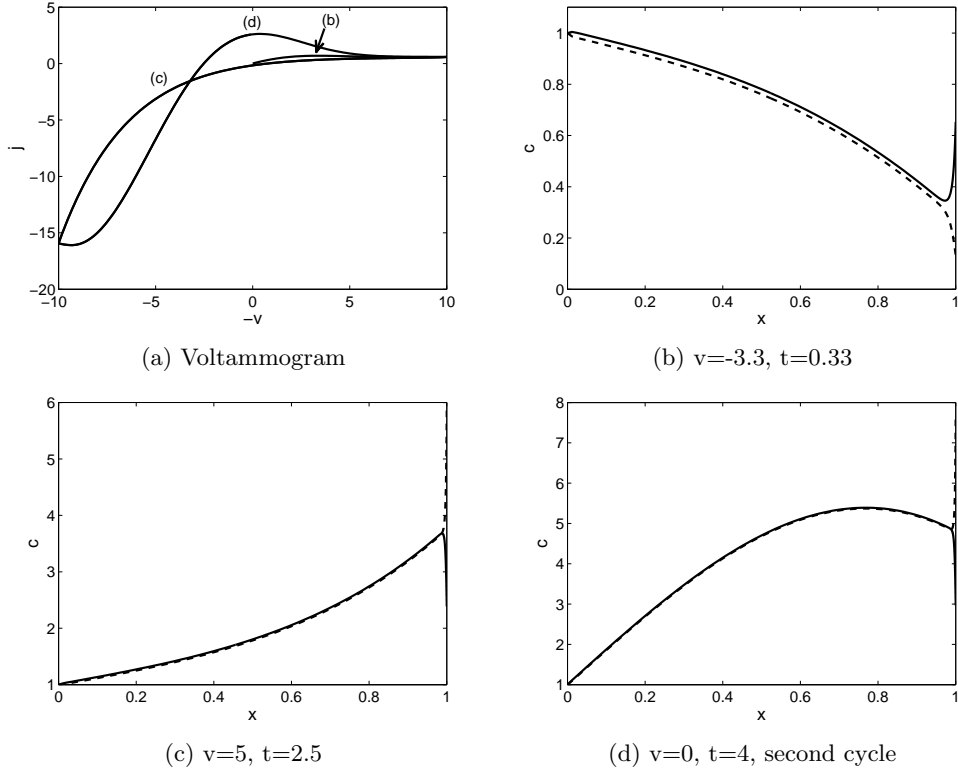


Figure 30: (a) Voltammogram and (b-d) resulting cation (solid line) and anion (dashed line) concentrations from a triangular applied voltage applied to a thin EDL liquid electrolyte with two electrodes and constant background charge. Parameters used were $\epsilon = 0.005$, $\delta = 1$, $k = 50$, $\rho_s = -0.01$ and $|\tilde{S}| = 10$. Two cycles are shown in Figure (a).

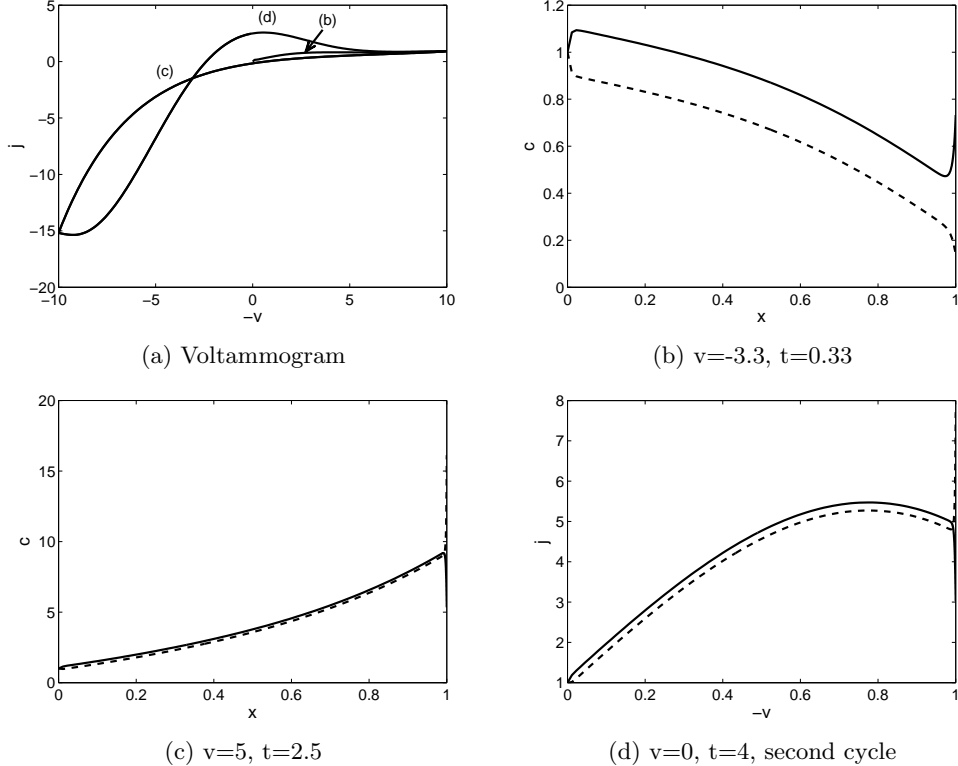


Figure 31: (a) Voltammogram and (b-d) resulting cation (solid line) and anion (dashed line) concentrations from a triangular applied voltage applied to a thin EDL liquid electrolyte with two electrodes and constant, negative background charge. Parameters used were $\epsilon = 0.005$, $\delta = 1$, $k = 50$, $\rho_s = -0.1$ and $|\tilde{S}| = 10$. Two cycles are shown in Figure (a).

Similar to the cyclic voltammogram in Section 4.3, the current-voltage relationship in Figures 30 and 31 displays diffusion limited behavior in the negative voltage sweep direction and purely exponential growth (reaction limiting behavior) in the other. This is because there is only one electrode in these simulations with only one of the two species taking part in the reaction. Furthermore, as with the space-charge voltammetry simulations in Section 6.4, the large voltage and fast sweep rate causes very large concentrations to develop near the electrodes (for example, $c_-(x = 1, t = 3) \approx 30$ in the $\rho_s = -0.01$ run). The addition of steric effects into the model would again be interesting here and make the results more realistic.

8.3. Positive Background Charge

For positive ρ_s , equation 57 predicts a decreasing current (or negative steady-state differential resistance) after the exponential portion, a behavior which has been observed in some experiments [31, 32] and not others [29]. Interestingly, when double-layer effects and electrode reaction kinetics are considered in the model simulations, the region of

negative resistance is also not observed, as shown in Figure 32 for $\rho_s = 0.01$ and in Figure 33 for $\rho_s = 0.1$. Physically, the interfaces provide overall positive differential resistance, even as the bulk charged electrolyte enters the over-limiting regime with negative local steady-state differential resistance.

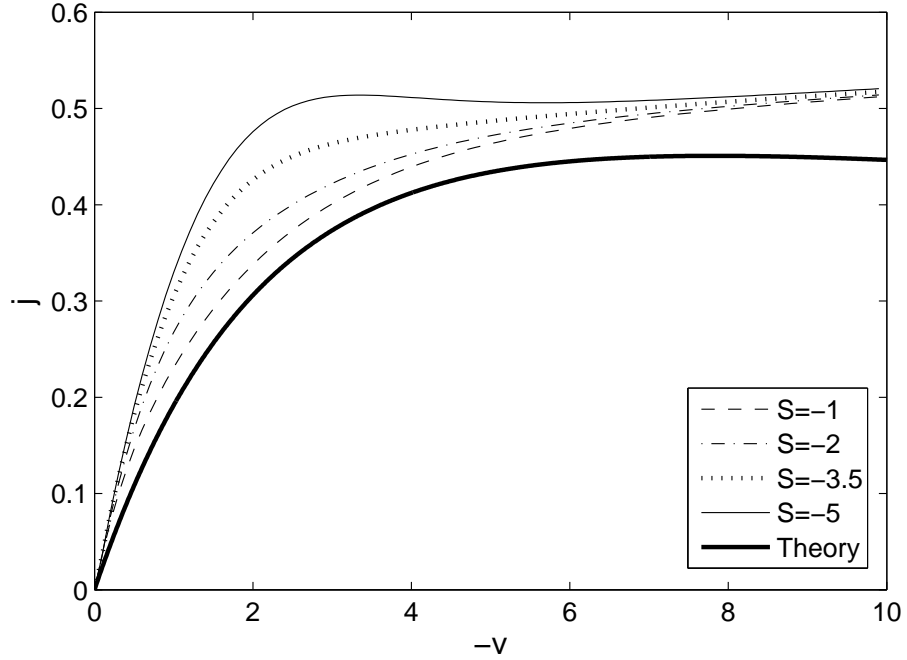


Figure 32: Current from a voltage ramp applied to a liquid electrolyte with a single electrode and constant, small, positive background charge. Parameters are $\epsilon = 0.005$, $\delta = 10$, $\rho_s = 0.01$ and $k = 50$. Also shown is the steady state response from equation (57), which is shown not to match the simulations.

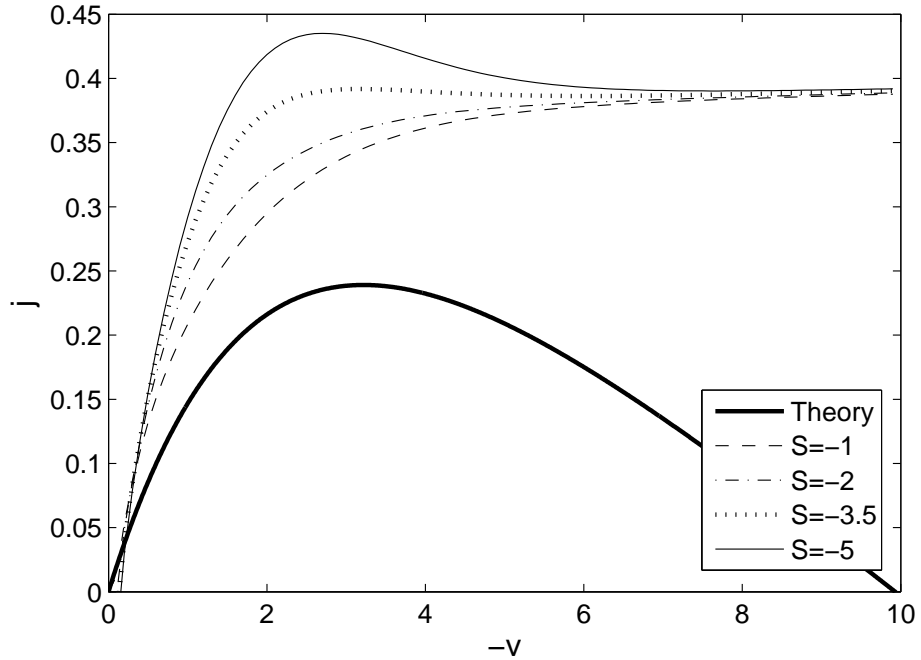


Figure 33: Current from a voltage ramp applied to a liquid electrolyte with a single electrode and constant, large, positive background charge. Parameters are $\epsilon = 0.005$, $\delta = 10$, $\rho_s = 0.1$ and $k = 50$. Also shown is the steady state response from equation (57), which is shown not to match the simulations

Finally, Figures 34 and 35 show voltammograms and concentrations for $\rho_s = 0.01$ and $\rho_s = 0.1$. For the concentrations shown for these two values of ρ_s , the difference between c_+ and c_- is $-2\rho_s$, which is -0.02 and -0.2 , respectively.

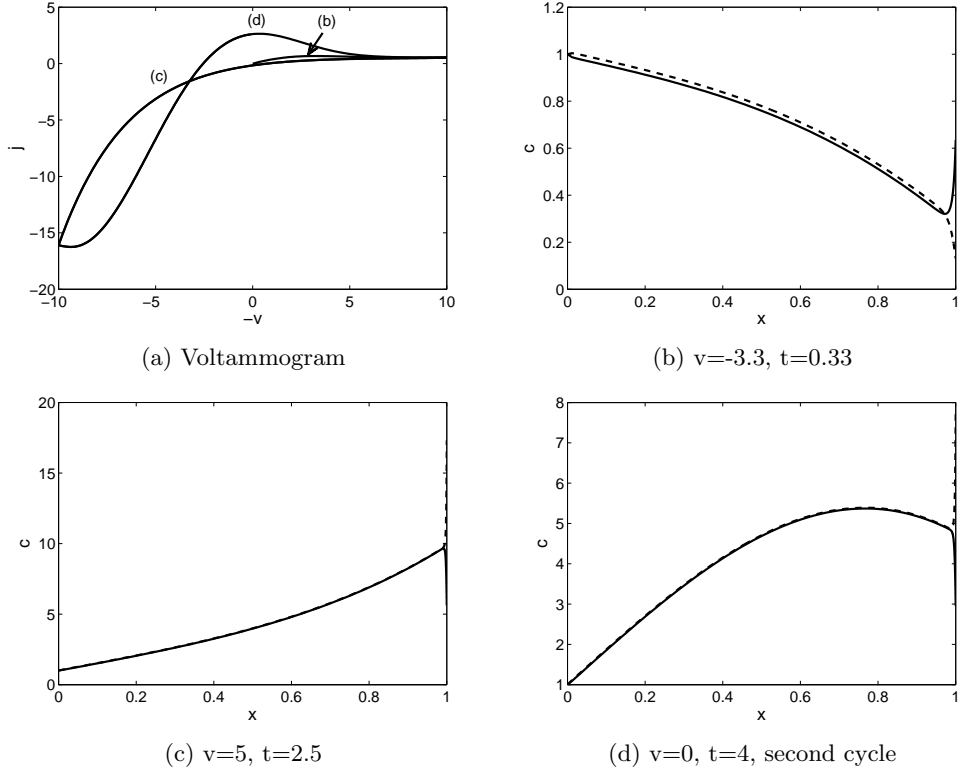


Figure 34: (a) Voltammogram and (b-d) resulting cation (solid line) and anion (dashed line) concentrations from a triangular applied voltage applied to a thin EDL liquid electrolyte with two electrodes and small positive background charge. Parameters used were $\epsilon = 0.005$, $\delta = 1$, $k = 50$, $\rho_s = 0.01$ and $|\tilde{S}| = 10$. Two cycles are shown in Figure (a).

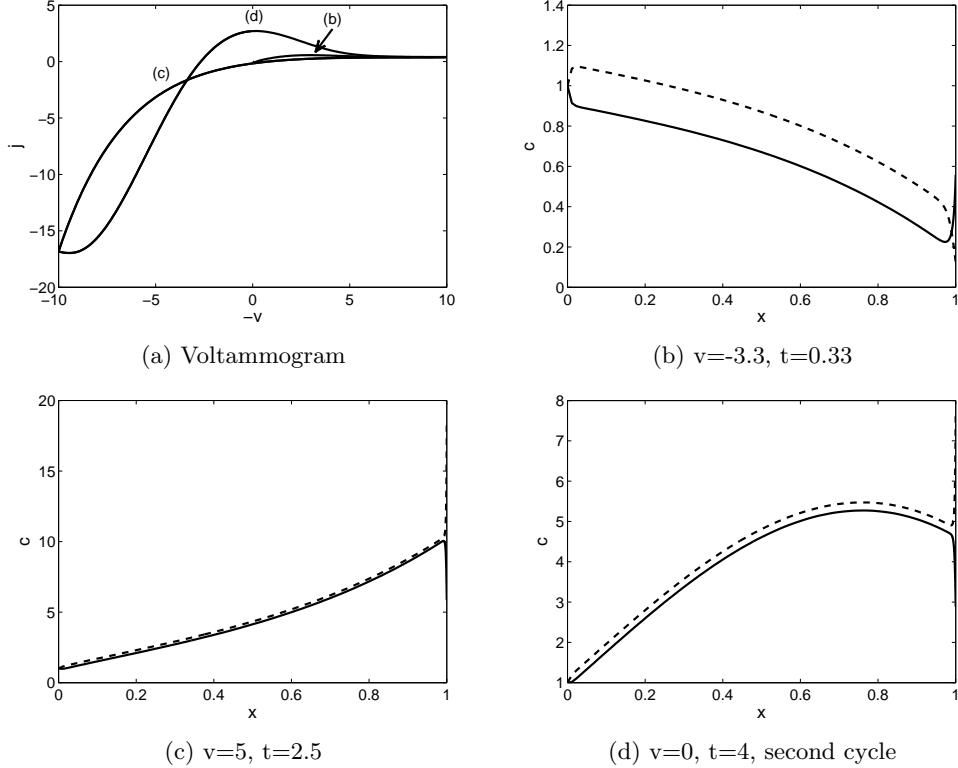


Figure 35: (a) Voltammogram and (b-d) resulting cation (solid line) and anion (dashed line) concentrations from a triangular applied voltage applied to a thin EDL liquid electrolyte with two electrodes and large positive background charge. Parameters used were $\epsilon = 0.005$, $\delta = 1$, $k = 50$, $\rho_s = 0.1$ and $|\tilde{S}| = 10$. Two cycles are shown in Figure (a).

9. Conclusions and Future Work

This paper provides a general theory to enable the use of LSV/CV to characterize electrochemical systems with diffuse charge. We first derived a theoretical current-voltage relation for voltammetry on a single electrode with fast reactions and showed how voltammetry in unsupported electrolytes differed from our modified Randles-Sevcik model. We then presented theory and simulations in a variety of situations which extend classical interpretations (unsupported liquid electrolytes and systems with blocking electrodes) and develop an understanding for more complicated situations (thin films, systems where bulk electroneutrality breaks down with space charge formation, and leaky membranes). Our simulation results were compared to limiting cases and we showed where simple analytical expressions can be used to predict behavior (such as approximating capacitance curves), and which regimes require more careful analysis and simulation. This is of practical interest for electrochemists and engineers, for whom it can assist in guiding the design of new devices and experiments.

For future work, there are many ways to extend the model for additional physics. For example, specific adoption of ions could be added to the boundary conditions, providing an additional mechanism for charge regulation of the surface [113, 114, 29], in addition to Faradaic polarization, coupled through the FBV equations. The PNP ion transport equations could be extended to include recombination bulk reactions (ion-ion, ion-defect, etc) [16] or various models of ion crowding effects [115, 105, 116, 81] or other non-idealities in concentrated solutions. There is also the possibility of coupled mass transport fluxes (Maxwell Stefan, dusty gas, etc) [117], which become important in concentrated electrolytes [7]. Poisson's equation could also be modified to account for electrostatic correlations [118] or dielectric polarization effects [119]. Furthermore, while we used generalized BV kinetics [96] in this work, Marcus kinetics [1, 120] may provide a more accurate model of charge transfer reactions. Even keeping the same PNP-FBV framework, it would be interesting to extend the model for 2d or 3d geometries, convection, and moving boundaries, in order to describe conversion batteries, electrodeposition and corrosion.

Appendix A. Derivation of Modified Randles-Sevcik Equation

In this appendix, we solve the semi-infinite diffusion equation with a nonhomogeneous boundary condition; the method is taken from Chapter 5.5 of O’Neil [121]. The equation and boundary conditions are

$$u_t = u_{xx} \quad (\text{A.1})$$

$$u(x, 0) = A \text{ for } x > 0 \quad (\text{A.2})$$

$$u(0, t) = f(t) \text{ (where } f(0) = A) \quad (\text{A.3})$$

We begin by considering the same problem with a jump at the boundary at time $t = t_0$:

$$u_t = u_{xx} \quad (\text{A.4})$$

$$u(x, 0) = A \text{ for } x > 0 \quad (\text{A.5})$$

$$u(0, t) = \begin{cases} A & 0 < t < t_0 \\ B & t > t_0 \end{cases} \quad (\text{A.6})$$

where A, B are positive constants. $u(0, t)$ can be written with the Heaviside step function $H(t)$ as

$$u(0, t) = A(1 - H(t - t_0)) + BH(t - t_0) \quad (\text{A.7})$$

The PDE (A.4)–(A.6) can be solved via Laplace transform. The Laplace transform of equation (A.4) is

$$sU(x, s) - A = \partial_{xx}U(x, s) \quad (\text{A.8})$$

where $U(x, s) = \mathcal{L}u(x, t)$. The general solution of equation (A.8), a constant-coefficient second order ODE for U , is

$$U(x, s) = a(s)e^{\sqrt{s}x} + b(s)e^{-\sqrt{s}x} + \frac{A}{s} \quad (\text{A.9})$$

We impose the condition $a(s) = 0$ because we would like the solution to be bounded as $x \rightarrow \infty$. This leaves us to solve for $b(s)$ using the boundary condition (equation (A.7)). The Laplace transform of equation (A.7) is

$$\mathcal{L}u(0, t) = \frac{A}{s} - \frac{A}{s}e^{-t_0s} + \frac{B}{s}e^{-t_0s} \quad (\text{A.10})$$

Using equation (A.10), $b(s)$ can be solved to be

$$b(s) = \frac{B - A}{s}e^{-t_0s} \quad (\text{A.11})$$

giving us

$$U(x, s) = \frac{B - A}{s}e^{-t_0s}e^{-\sqrt{s}x} + \frac{A}{s} \quad (\text{A.12})$$

We can now take the inverse Laplace transform of equation (A.12) to obtain

$$u(x, t) = A + (B - A) \operatorname{erfc} \left(\frac{x}{2\sqrt{t - t_0}} \right) \quad (\text{A.13})$$

where $\operatorname{erfc}(z) = 1 - \operatorname{erf}(z) = \frac{2}{\sqrt{\pi}} \int_z^\infty \exp(-x^2) dx$ is the complementary error function. In other words, the solution to the semi-infinite diffusion problem with a jump of $\Delta u(0, t_0)$ relative to A at $x = 0$ and time $t = t_0$ is

$$u(x, t) = A + \Delta u(0, t_0) \operatorname{erfc} \left(\frac{x}{2\sqrt{t - t_0}} \right) \quad (\text{A.14})$$

Now, using Duhamel's principle, we have for an arbitrary series of steps at $t = t_i$ given by $\Delta u(0, t_i) = f(t_i)$,

$$u(x, t) = A + \sum_i \Delta f(t_i) \operatorname{erfc} \left(\frac{x}{2\sqrt{t - t_i}} \right) \quad (\text{A.15})$$

where $\Delta f(t_i) = f(t_{i+1}) - f(t_i)$. We can take the continuum limit with $\Delta f(t_i) = \frac{df}{dt}(\tilde{t}_i) \Delta t_i$, where $t_i < \tilde{t}_i < t_{i+1}$ to obtain

$$u(x, t) = A + \int_0^t \frac{df}{dt}(t') \operatorname{erfc} \left(\frac{x}{2\sqrt{t - t'}} \right) dt' \quad (\text{A.16})$$

and finally we can make the substitution $\tau = t - t'$ to write

$$\begin{aligned} u(x, t) &= A - \int_t^0 \frac{df}{dt}(t - \tau) \operatorname{erfc} \left(\frac{x}{2\sqrt{\tau}} \right) d\tau \\ &= A + \int_0^t \frac{df}{dt}(t - \tau) \operatorname{erfc} \left(\frac{x}{2\sqrt{\tau}} \right) d\tau \end{aligned} \quad (\text{A.17})$$

Equation (A.17) may be numerically integrated. Alternatively, if we are interested in the Nernstian function, $f(t) = e^{-St}$ (for quasi-equilibrium fast reactions, as in equation (24)) and wish to compute the resulting current $j = u_x(0, t)$, we can arrive at an analytical expression for $u_x(0, t)$,

$$u_x(x, t) = S e^{-St} \int_0^t \frac{e^{S\tau} e^{-\frac{x^2}{4\tau}}}{\sqrt{\pi\tau}} d\tau \quad (\text{A.18})$$

$$u_x(0, t) = \sqrt{S} e^{-St} \operatorname{erfi} \left(\sqrt{St} \right) \quad (\text{A.19})$$

where $\operatorname{erfi}(z) = \frac{2}{\sqrt{\pi}} \int_0^z \exp(-x^2) dx$ is the imaginary error function.

References

References

[1] A. J. Bard, L. R. Faulkner, *Electrochemical Methods: Fundamentals and Applications*, John Wiley & Sons, New York, 2001.

- [2] R. G. Compton, C. E. Banks, *Understanding Voltammetry*, Imperial College Press, London, 2011.
- [3] R. G. Compton, E. Laborda, K. R. Ward, *Understanding Voltammetry: Simulation of Electrode Processes*, Imperial College Press, London, 2014.
- [4] J. E. B. Randles, Kinetics of rapid electrode reactions, *Discussions of the Faraday Society* 1 (1947) 11–19.
- [5] J. E. B. Randles, A cathode ray polarograph. part II. The current-voltage curves, *Trans. Faraday Soc.* 44 (1948) 327–338.
- [6] A. Sevcik, Oscillographic polarography with periodical triangular voltage, *Collection of Czechoslovak Chemical Communications* 13 (1948) 349–377.
- [7] J. Newman, K. E. Thomas-Alyea, *Electrochemical Systems*, John Wiley & Sons, Hoboken, NJ, 2012.
- [8] P. Simon, Y. Gogotsi, Materials for electrochemical capacitors, *Nature Materials* 7 (11) (2008) 845–854.
- [9] P. M. Biesheuvel, M. Z. Bazant, Nonlinear dynamics of capacitive charging and desalination by porous electrodes, *Phys. Rev. E* 81 (3) (2010) 031502.
- [10] P. M. Biesheuvel, Y. Fu, M. Z. Bazant, Diffuse charge and Faradaic reactions in porous electrodes, *Phys. Rev. E* 83 (6) (2011) 061507.
- [11] P. M. Biesheuvel, Y. Fu, M. Z. Bazant, Electrochemistry and capacitive charging of porous electrodes in asymmetric multicomponent electrolytes, *Russian J. Electrochem.* 48 (6) (2012) 580–591.
- [12] M. Z. Bazant, K. T. Chu, B. J. Bayly, Current-voltage relations for electrochemical thin films, *SIAM J. Appl. Math.* 65 (5) (2005) 1463–1484.
- [13] K. T. Chu, M. Z. Bazant, Electrochemical thin films at and above the classical limiting current, *SIAM J. Appl. Math.* 65 (5) (2005) 1485–1505.
- [14] P. M. Biesheuvel, M. van Soestbergen, M. Z. Bazant, Imposed currents in galvanic cells, *Electrochimica Acta* 54 (2009) 4857–4871.
- [15] M. van Soestbergen, Frumkin-butler-volmer theory and mass transfer in electrochemical cells, *Russian Journal of Electrochemistry* 48 (6) (2012) 570–579.
- [16] A. C. Luntz, J. Voss, K. Reuter, Interfacial challenges in solid-state Li Ion batteries, *J. Phys. Chem. Lett.* 6 (22) (2015) 4599–4604.
- [17] J.-M. Tarascon, M. Armand, Issues and challenges facing rechargeable lithium batteries, *Nature* 414 (6861) (2001) 359–367.
- [18] R. Muralidhar, T. Shaw, F. Chen, P. Oldiges, D. Edelstein, S. Cohen, R. Achanta, G. Bonilla, M. Bazant, TDDB at low voltages: An electrochemical perspective, in: 2014 IEEE International Reliability Physics Symposium, 2014.
- [19] P. M. Biesheuvel, A. A. Franco, M. Z. Bazant, Diffuse charge effects in fuel cell membranes, *J. Electrochem. Soc.* 156 (2) (2009) B225–B233.
- [20] A. A. Franco, P. Schott, C. Jallut, B. Maschke, A multi-scale dynamic mechanistic model for the transient analysis of PEFCs, *Fuel Cells* 7 (2) (2007) 99–117.
- [21] M. Z. Bazant, T. M. Squires, Induced-charge electrokinetic phenomena: theory and microfluidic applications, *Phys. Rev. Lett.* 92 (6) (2004) 066101.
- [22] T. M. Squires, S. R. Quake, Microfluidics: Fluid physics at the nanoliter scale, *Rev. Modern Phys.* 77 (3) (2005) 977.
- [23] R. B. Schoch, J. Han, P. Renaud, Transport phenomena in nanofluidics, *Rev. Modern Phys.* 80 (3) (2008) 839.
- [24] I. Rubinstein, L. Shtilman, Voltage against current curves of cation exchange membranes, *J. Chem. Soc.* 75 (1979) 231–246.
- [25] I. Rubinstein, E. Staude, O. Kedem, Role of the membrane surface in concentration polarization at ion-exchange membrane, *Desalination* 69 (2) (1988) 101–114.
- [26] V. V. Nikonenko, N. D. Pismenskaya, E. I. Belova, P. Sistat, P. Huguet, G. Pourcelly, C. Larchet, Intensive current transfer in membrane systems: Modelling, mechanisms and application in electrodialysis, *Adv. Colloid Interface Sci.* 160 (1) (2010) 101–123.
- [27] E. V. Dydek, B. Zaltzman, I. Rubinstein, D. S. Deng, A. Mani, M. Z. Bazant, Overlimiting current in a microchannel, *Phys. Rev. Lett.* 107 (11) (2011) 118301.
- [28] E. V. Dydek, M. Z. Bazant, Nonlinear dynamics of ion concentration polarization in porous media: The leaky membrane model, *AIChE Journal* 59 (9) (2013) 3539–3555.
- [29] D. Deng, E. V. Dydek, J.-H. Han, S. Schlumpberger, A. Mani, B. Zaltzman, M. Z. Bazant, Overlimiting current and shock electrodialysis in porous media, *Langmuir* 29 (52) (2013) 16167–16177.
- [30] S. Schlumpberger, N. B. Lu, M. E. Suss, M. Z. Bazant, Scalable and continuous water deionization

by shock electrodialysis, *Environ. Sci. Technol. Lett.* 2 (12) (2015) 367–372.

[31] J.-H. Han, E. Khoo, P. Bai, M. Z. Bazant, Over-limiting current and control of dendritic growth by surface conduction in nanopores, *Sci. Rep.* 4.

[32] J. H. Han, M. Wang, P. Bai, F. R. Brushett, M. Z. Bazant, Dendrite suppression by shock electrodeposition in charged porous media, *Sci. Rep.* 6 (2016) 28054.

[33] E. Itskovich, A. A. Kornyshev, M. A. Vorotyntsev, Electric current across the metal-solid electrolyte interface i. direct current, current-voltage characteristic, *Physica Status Solidi A* 39 (1) (1977) 229–238.

[34] A. A. Kornyshev, M. A. Vorotyntsev, Conductivity and space charge phenomena in solid electrolytes with one mobile charge carrier species, a review with original material, *Electrochimica Acta* 26 (3) (1981) 303–323.

[35] A. Bonnefont, F. Argoul, M. Z. Bazant, Analysis of diffuse-layer effects on time-dependent interfacial kinetics, *J. Electroanal. Chem.* 500 (2001) 52–61.

[36] R. He, S. Chen, F. Yang, B. Wu, Dynamic diffuse double-layer model for the electrochemistry of nanometer-sized electrodes, *J. Phys. Chem. B* 110 (7) (2006) 3262–3270.

[37] I. Streeter, R. G. Compton, Numerical simulation of potential step chronoamperometry at low concentrations of supporting electrolyte, *J. Phys. Chem. C* 112 (35) (2008) 13716–13728.

[38] M. Z. Bazant, K. Thornton, A. Ajdari, Diffuse-charge dynamics in electrochemical systems, *Phys. Rev. E* 70 (2) (2004) 021506.

[39] A. Frumkin, Wasserstoffüberspannung und structur der doppelschicht, *Z. Phys. Chem.* 164A (1933) 121–133.

[40] V. G. Levich, Theory of the nonequilibrium double layer, *Dokl. Akad. Nauk SSSR* 67 (1949) 309.

[41] E. Barsoukov, J. R. Macdonald, *Impedance Spectroscopy: Theory, Experiment, and Applications*, Wiley, Hoboken, 2005.

[42] G. Jaffé, *Ann. Phys.* 16 (1933) 249.

[43] G. Jaffé, Theory of conductivity of semiconductors, *Phys. Rev.* 85 (2) (1952) 354–363.

[44] H.-C. Chang, G. Jaffé, *Polarization in Electrolytic Solutions. Part I. Theory*, Vol. 20, 1952.

[45] J. R. Macdonald, Theory of spacecharge polarization and electrodedischarge effects, *J. Chem. Phys.* 58 (11) (1973) 4892–5001.

[46] J. R. Macdonald, D. R. Franceschetti, Theory of smallsignal ac response of solids and liquids with recombining mobile charge, *J. Chem. Phys.* 68 (4) (1978) 1614–1637.

[47] J. R. Macdonald, Effects of Chang-Jaffe and other boundary conditions on the response of Poisson-Nernst-Planck impedance spectroscopy analysis models and correlation with the CTRW UN model, *J. Phys. Chem. A* 115 (46) (2011) 13370–13380.

[48] J. D. Jackson, *Classical Electrodynamics*, Wiley, New York, 1962.

[49] M. van Soestbergen, P. M. Biesheuvel, M. Z. Bazant, Diffuse-charge effects on the transient response of electrochemical cells, *Phys. Rev. E* 81 (2) (2010) 1–13.

[50] R. P. Buck, Steady-state space charge effects in symmetric cells with concentration polarized electrodes, *Journal of Electroanalytical Chemistry and Interfacial Electrochemistry* 46 (1) (1973) 1–23.

[51] J. D. Norton, H. S. White, S. W. Feldberg, Effect of the electrical double layer on voltammetry at microelectrodes, *J. Phys. Chem.* 94 (17) (1990) 6772–6780.

[52] W. . Murphy, J. A. Manzanares, S. . Mafe, H. Reiss, A numerical study of the equilibrium and nonequilibrium diffuse double layer in electrochemical cells, *J. Phys. Chem.* 96 (24) (1992) 9983–9991.

[53] C. P. Smith, H. S. White, Theory of the voltammetric response of electrodes of submicron dimensions. violation of electroneutrality in the presence of excess supporting electrolyte, *Anal. Chem.* 65 (23) (1993) 3343–3353.

[54] K. B. Oldham, A. M. Bond, How valid is the electroneutrality approximation in the theory of steady-state voltammetry?, *J. Electroanal. Chem.* 508 (1) (2001) 28–40.

[55] A. M. Bond, M. Fleischmann, J. Robinson, Electrochemistry in organic solvents without supporting electrolyte using platinum electrodes, *J. Electroanal. Chem.* 168 (1) (1984) 299–312.

[56] A. M. Bond, P. A. Lay, Cyclic voltammetry at microelectrodes in the absence of added electrolyte using a platinum quasi-reference electrode, *J. Electroanal. Chem.* 199 (2) (1985) 285–295.

[57] A. M. Bond, D. C. Coomber, S. W. Feldberg, K. B. Oldham, T. Vu, An experimental evaluation of cyclic voltammetry of multicharged species at macrodisk electrodes in the absence of added supporting electrolyte, *Anal. Chem.* 73 (2) (1984) 352–359.

[58] A. M. Bond, M. Fleischmann, J. Robinson, Voltammetric measurements using microelectrodes in highly dilute solutions, *J. Electroanal. Chem.* 172 (1–2) (1984) 11–25.

[59] K. B. Oldham, Theory of microelectrode voltammetry with little electrolyte, *J. Electroanal. Chem.* 250 (1) (1998) 1–21.

[60] J. C. Myland, K. B. Oldham, Limiting currents in potentiostatic voltammetry without supporting electrolyte, *Electrochemistry communications* 1 (10) (1999) 467–471.

[61] K. B. Oldham, S. W. Feldberg, Principle of unchanging total concentration and its implication for modeling unsupported transient voltammetry, *J. Phys. Chem. B* 103 (10) (1999) 1699–1704.

[62] K. B. Oldham, F. Marken, J. C. Myland, Theory of unsupoprted, steady-state, Nernstian, three-ion, twin-electrode, voltammetry: the special case of dual concentration polarization, *J. Solid State. Electrochem.* (2016) 1–13.

[63] M. F. Bento, L. Thouin, C. Amatore, M. I. Montenegro, About potential measurements in steady state voltammetry at low electrolyte/analyte concentration ratios, *J. Electroanal. Chem.* 443 (1) (1998) 137–148.

[64] C. Amatore, L. Thouin, M. F. Bento, Steady state voltammetry at low electrolyte/reactant concentration ratios: what it means and what it does not mean, *J. Electroanal. Chem.* 463 (1) (1999) 45–52.

[65] M. F. Bento, L. Thouin, C. Amatore, Potential measurements in steady state voltammetry at low electrolyte/analyte concentration ratios. role of convection on ohmic drop: a simplified model, *J. Electroanal. Chem.* 446 (1) (1998) 91–105.

[66] E. J. F. Dickinson, R. G. Compton, Influence of the diffuse double layer on steady-state voltammetry, *J. Electroanal. Chem.* 661 (1) (2011) 192–212.

[67] E. J. F. Dickinson, J. G. Limon-Petersen, R. G. Compton, The electroneutrality approximation in electrochemistry, *J. Solid State Electrochem.* 15 (7–8) (2011) 1335–1345.

[68] C. Batchelor-McAuley, E. Kätelhön, E. O. Barnes, R. G. Compton, E. Laborda, A. Molina, Recent advances in voltammetry, *ChemistryOpen* 4 (3) (2015) 224–260.

[69] E. J. F. Dickinson, R. G. Compton, The zero-field approximation for weakly supported voltammetry: A critical evaluation, *Chem. Phys. Lett.* 497 (4) (2010) 178–183.

[70] S. R. Belding, R. G. Compton, Cyclic voltammetry in the absence of excess supporting electrolyte: the effect of analyte charge, *J. Electroanal. Chem.* 683 (2012) 1–13.

[71] J. G. Limon-Petersen, I. Streeter, N. V. Rees, R. G. Compton, Voltammetry in weakly supported media: the stripping of thallium from a hemispherical amalgam drop. theory and experiment, *J. Phys. Chem. C* 112 (44) (2008) 17175–17182.

[72] J. G. Limon-Petersen, I. Streeter, N. V. Rees, R. G. Compton, Quantitative voltammetry in weakly supported media: effects of the applied overpotential and supporting electrolyte concentration on the one electron oxidation of ferrocine in acetonitrile, *J. Phys. Chem. C* 113 (1) (2009) 333–337.

[73] S. R. Belding, J. G. Limon-Petersen, E. J. F. Dickinson, R. G. Compton, Cyclic voltammetry in the absence of excess supporting electrolyte offers extra kinetic and mechanistic insights: Comproportionation of anthraquinone and anthraquinone dianion in acetonitrile, *Angewandte Chemie International Edition* 49 (48) (2010) 9242–9245.

[74] E. J. F. Dickinson, J. G. Limon-Petersen, N. V. Rees, R. G. Compton, How much supporting electrolyte is required to make a cyclic voltammetry experiment quantitatively “diffusional”? a theoretical and experimental investigation, *J. Phys. Chem. C* 113 (35) (2009) 11157–11171.

[75] K. Aoki, Theory of ultramicroelectrodes, *Electroanalysis* 5 (8) (1993) 627–639.

[76] O. Stern, Zur theorie der elektrolytischen doppelschicht, *Z. Electrochem.* 30 (1924) 508–516.

[77] L. H. Olesen, M. Z. Bazant, H. Bruus, Strongly nonlinear dynamics of electrolytes in large ac voltages, *Phys. Rev. E* 82 (1) (2010) 011501.

[78] M. van Soestbergen, Ionic currents exceeding the diffusion limitation in planar nano-cavities, *Electrochemistry Communications* 20 (2012) 105–108.

[79] M. Zevenbergen, B. Wolfrum, E. Goluch, P. Singh, S. Lemay, Fast electron-transfer kinetics probed in nanofluidic channels, *J. Am. Chem. Soc.* 131 (32) (2009) 11471–11477.

[80] M. Zevenbergen, P. Singh, E. Goluch, B. Wolfrum, S. Lemay, Electrochemical correlation spectroscopy in nanofluidic cavities, *Anal. Chem.* 81 (19) (2009) 8203.

[81] M. Z. Bazant, M. S. Kilic, B. D. Storey, A. Ajdari, Towards an understanding of induced-charge electrokinetics at large applied voltages in concentrated solutions, *Advances in colloid and interfacial science* 152 (1) (2009) 48–88.

[82] L. H. Olesen, H. Bruus, A. Ajdari, AC electrokinetic micropumps: the effect of geometrical confinement, Faradaic current injection, and nonlinear surface capacitance, *Phys. Rev. E* 73 (5) (2006) 056313.

[83] L. H. Olesen, AC electrokinetic micropumps, Ph.D. thesis, Danish Technical University (2006).

[84] J. L. Moran, J. D. Posner, Electrokinetic locomotion due to reaction-induced-charge auto-

electrophoresis, *J. Fluid Mech.* 680 (2011) 31–66.

[85] J. L. Moran, P. M. Wheat, J. D. Posner, Locomotion of electrocatalytic nanomotors due to reaction induced charge autoelectrophoresis, *Phys. Rev. E* 81 (6) (2010) 065302.

[86] B. M. Grafov, A. A. Cherenko, Theory of the passage of a constant current through a solution of a binary electrolyte, *Dokl. Akad. Nauk. SSSR* 146 (1962) 135–138, English translation, pp. 629–632.

[87] J. Newman, W. H. Smyrl, The polarized diffuse double layer, *Trans. Faraday Soc.* 61 (1965) 2229–2237.

[88] W. H. Smyrl, J. Newman, Double layer structure at the limiting current, *Trans. Faraday Soc.* 63 (1966) 207–216.

[89] A. D. MacGillivray, Nernst-Planck equations and the electroneutrality and Donnan equilibrium assumptions, *J. Chem. Phys.* 48 (7) (1968) 2903–2907.

[90] I. Rubinstein, B. Zaltzman, Electro-osmotic slip of the second kind and instability in concentration polarization at electrodialysis membranes, *Math. Mod. Meth. Appl. Sci.* 11 (2001) 263–300.

[91] B. Zaltzman, I. Rubinstein, Electro-osmotic slip and electroconvective instability, *Journal of Fluid Mechanics* 579 (2007) 173–226.

[92] D. R. Baker, M. W. Verbrugge, The role of charge separation in the response of electrochemical systems, *Proc. R. Soc. London A* 454 (1975) (1997) 1805–1829.

[93] G. Richardson, J. R. King, Time-dependent modelling and asymptotic analysis of electrochemical cells, *J. Eng. Math.* 59 (3) (2007) 239–275.

[94] A. A. Moya, E. Belashova, P. Sistat, Numerical simulation of linear sweep and large amplitude AC voltammetries of ion-exchange membrane systems, *J. Membrane Sci.* 474 (2015) 215–223.

[95] T. B. Grimley, N. F. Mott, I. general and theoretical. the contact between a solid and a liquid electrolyte, *Discussions of the Faraday Soc.* 1 (1947) 3–11.

[96] M. Z. Bazant, Theory of chemical kinetics and charge transfer based on nonequilibrium thermodynamics, *Accounts of Chemical Research* 46 (5) (2013) 1144–1160.

[97] D. Wang, S. J. Ruuth, Variable step-size implicit-explicit linear multistep methods for time-dependent partial differential equations, *Journal of Computational Mathematics* 26 (6) (2008) 838–855.

[98] U. M. Ascher, S. J. Ruuth, B. T. R. Wetton, Implicit-explicit methods for time-dependent partial differential equations, *SIAM Journal on Numerical Analysis* 32 (3) (1995) 797–823.

[99] M. Gouy, Sur la constitution de la charge électrique à la surface d'un électrolyte, *J. Phys. Theor. Appl.* (1910) 457–468.

[100] D. L. Chapman, A contribution to the theory of electrocapillarity, *Phil. Mag.* 25 (148) (1913) 475–481.

[101] A. A. Lee, S. Kondrat, G. Oshanin, A. A. Kornyshev, Charging dynamics of supercapacitors with narrow cylindrical nanopores, *Nanotechnology* 25 (31) (2014) 315401.

[102] S. Porada, R. Zhao, A. van der Wal, V. Presser, P. M. Biesheuvel, Review on the science and technology of water desalination by capacitive deionization, *Progress in Materials Science* 58 (8) (2013) 1388–1442.

[103] R. Zhao, P. M. Biesheuvel, A. van der Wal, Energy consumption and constant current operation in membrane capacitive deionization, *Energy & Environmental Science* 5 (11) (2012) 9520–9527.

[104] M. Z. Bazant, T. M. Squires, Induced-charge electrokinetic phenomena, *Current Opinion in Colloid & Interface Science* 15 (3) (2010) 203–213.

[105] M. S. Kilic, M. Z. Bazant, A. Ajdari, Steric effects in the dynamics of electrolytes at large applied voltages. II. Modified Poisson-Nernst-Planck equations, *Phys. Rev. E* 75 (2).

[106] T. Teorell, An attempt to formulate a quantitative theory of membrane permeability, *Experimental Biology and Medicine* 33 (2) (1935) 282–285.

[107] K. H. Meyer, J. F. Sievers, La perméabilité des membranes, *Helv. Chem. Acta* 19 (1) (1936) 649–664.

[108] K. S. Spiegler, Polarization at ion exchange membrane-solution interfaces, *Desalination* 9 (4) (1971) 367–385.

[109] R. Abu-Rjhal, V. Chinaryan, M. Z. Bazant, I. Rubinstein, B. Zaltzman, Effect of concentration polarization on perm-selectivity, *Phys. Rev. E* 89 (1) (2014) 012302.

[110] A. Yaroshchuk, Over-limiting currents and deionization shocks in current-induced polarization: local equilibrium analysis, *Adv. Colloid Interface Sci.* 183 (2012) 68–81.

[111] A. Mani, M. Z. Bazant, Deionization shocks in microstructures, *Phys. Rev. E* 84 (6) (2011) 061504.

[112] P. B. Peters, R. van Roij, M. Z. Bazant, P. M. Biesheuvel, Analysis of electrolyte transport through charged nanopores, *Phys. Rev. E* 93 (2016) 053108.

[113] C. Gentil, D. Côte, U. Bockelmann, Transistor based study of the electrolyte/SiO₂ interface, *Phys.*

Stat. Sol. A 203 (14) (2006) 3412–3416.

- [114] S. H. Behrens, D. G. Grier, The charge of glass and silica surfaces, *J. Chem. Phys.* 115 (14) (2001) 6716–6721.
- [115] M. S. Kilic, M. Z. Bazant, A. A. I. Double-layer charging, Steric effects in the dynamics of electrolytes at large applied voltages, *Phys. Rev. E* 75 (2).
- [116] A. A. Kornyshev, Double-layer in ionic liquids: Paradigm change?, *J. Phys. Chem. B* 111 (2007) 5545–5557.
- [117] R. Taylor, R. Krishna, *Multicomponent Mass Transfer*, Wiley, New York, 1993.
- [118] M. Z. Bazant, B. D. Storey, A. A. Kornyshev, Double layer in ionic liquids: Overscreening versus crowding, *Phys. Rev. Lett.* 106 (4) (2011) 046102.
- [119] M. M. Hatlo, R. V. Roij, L. Lue, The electric double layer at high surface potentials: The influence of excess ion polarizability, *Europhys. Lett.* 97 (2) (2012) 28010.
- [120] Y. Zeng, R. B. Smith, P. Bai, M. Z. Bazant, Simple formula for marcus-hush-chidsey kinetics, *J. Electroanal. Chem.* 753 (2014) 77–83.
- [121] P. V. O’Neil, *Beginning Partial Differential Equations*, 3rd ed., Wiley, Hoboken, 2008.